Optimising Chemotherapy for Advanced High-Grade Serous Ovarian Cancer via Delay-Differential Equations

Cristina Koprinski[1, *, †], Georgio Hawi[1, †], and Peter S. Kim[1]

[1]School of Mathematics and Statistics, University of Sydney, Sydney, Australia
[*]Corresponding author: cristina.koprinski@sydney.edu.au
[†]These authors contributed equally to this work

Abstract

Ovarian cancer is the deadliest gynaecological cancer and the fourth leading cause of cancer deaths in women. High-grade serous ovarian cancer (HGSOC) accounts for 75% of cases, and chemotherapy resistance and relapse occur in 85% of patients, leading to a 5-year survival of 45%. Currently, the literature lacks comprehensive immunobiological models of HGSOC, and developing such models could provide critical insights into the disease's underlying mechanisms and interactions within the tumour microenvironment. We address this by constructing an immunobiological model using delay differential equations and then optimise chemotherapy regimens to maximise efficacy, minimise toxicity, and improve treatment efficiency for first-line treatment. The model consists of two compartments, the tumour site and tumour-draining lymph node, with immune processes such as DC maturation, T cell priming and proliferation, and cytokine interactions modelled. Parameter values are estimated using experimental data from ovarian cancer tissue samples as well as the TCGA OV database. The results indicate that low-dose dose more frequent chemotherapy provides comparable results to the standard regimen with a lower toxicity, and alternative dosing strategies with rest weeks can allow patients to recover from the toxic side effects of chemotherapy.

1 Introduction

High-grade serous ovarian cancer (HGSOC) is the most common subtype of ovarian cancer and the fourth leading cause of cancer-related deaths in women worldwide, with a 5-year survival rate of 45% [1]. Its poor prognosis is partly due to asymptomatic early stages and a lack of screening programs, resulting in approximately 80% of cases being diagnosed at Stages III or IV [2]. At the same time, 70–80% of HGSOC patients experience recurrence after primary surgery and resistance to initial chemotherapy, contributing to poor long-term survival outcomes [3–5]. Of new HGSOC cases, half of the diagnoses occur in women over 64, and the disease burden is expected to increase due to ageing populations and increased life expectancy [6].

The primary first-line treatment for patients with HGSOC is neoadjuvant chemotherapy (NACT) followed by surgery or adjuvant chemotherapy (ACT) after surgery aimed at removing all visible tumours within the peritoneal cavity, with the degree of cytoreduction being a critical prognostic factor [7, 8]. Randomised clinical trials, including EORTC 55971, CHORUS, JCOG0602, and SCORPION-NCT01461850, have shown no significant difference in overall survival and progression-free survival

(PFS) between NACT and ACT in ovarian cancer [9–12]. However, in advanced cancer, NACT is preferred due to its potential to facilitate increased rates of optimal cytoreduction [13, 14]. The standard chemotherapy regimen (SR) has been the combination of paclitaxel (175 mg/m^2; 3h infusion) and carboplatin (AUC 5 or 6; 30 min infusion), administered intravenously every three weeks for three/-four cycles in the NACT and five/six cycles in ACT [9, 15–17]. Trials in the mid-1990s established that this regimen is superior to cisplatin and cyclophosphamide [18, 19], with later studies confirming that substituting cisplatin for carboplatin offers similar efficacy with improved safety [20, 21]. The SR dosing is based on the principle that higher doses increase the effectiveness of cancer cell eradication while maintaining tolerability [22, 23]. While aiming to maximise tumour depletion, chemotherapy's cytotoxic effects on healthy tissues and high toxicity, including neurotoxicity, require prolonged rest periods and impair patients' quality of life [24].

In the past decade, there has been growing interest in alternative dosing, including more frequent, low-dose drug administrations (dose-dense and metronomic therapies), due to their potential efficacy and low toxicity in various cancers [25]. In the Japanese JGOG3016 trial, patients with Stage II, III and IV epithelial ovarian cancer were randomised to receive triweekly carboplatin (AUC 6) and weekly paclitaxel (80 mg/m^2), or the SR, with results showing significantly improved PFS compared to the SR [26]. However, the GOG-0262 trial, which trialled the same regime in a European population, did not find a significantly improved PFS to the SR [27]. Separately, a metronomic dosing regimen of weekly carboplatin (AUC 2) and paclitaxel (60 mg/m^2) was trialled in elderly patients in the MITO-5 trial, concluding comparable results to the SR with reduced toxicity, and was further supported by the MITO-7 trial in a larger cohort [28, 29]. This prompted the ICON8 study, which found comparable results to the SR for both these dosing regimens; however, as no significant improvement in PFS was observed, the SR remains the standard of care in European populations [30]. Despite this, dose-dense and metronomic regimens remain useful for patients who cannot tolerate the SR, such as elderly and vulnerable patients [31].

An important question is the appropriate dosing and spacing of paclitaxel and carboplatin therapies to balance tumour reduction with factors such as toxicity and efficacy. This can be achieved through the construction of immunobiological mathematical models and has been employed in cancers such as colorectal, breast and pancreatic to optimise chemotherapy and other treatment regimens [32–34]. These models also provide insights into the underlying biological processes guiding further research and clinical trials [35]. Our work builds on [36] and [37] by applying a two-compartment model, incorporating the tumour site (TS) and the tumour-draining lymph node (TDLN), to HGSOC and chemotherapy. This enables more accurate modelling of immune cell types and interactions, such as antigen presentation and cell proliferation in the TDLN. To the authors' knowledge, no existing mathematical models in the literature consider the immunobiology of HGSOC with paclitaxel and carboplatin. Few related models exist, the first by Panetta who used a two-compartment model of proliferating and quiescent cancer cells to investigate the effect of varying dosages and infusion times of paclitaxel, and the second by Kohandel et al. who expanded this model to investigate the effectiveness of NACT and ACT therapies [38, 39]. Although these models provide a modelling foundation, they do not incorporate the role of various immune cells and cytokines in the TME, opting to only consider the cancer cell concentration over time.

Hence, it is important to briefly outline the functions of immune cells and cytokines in the tumour microenvironment (TME), as their interaction with cancer cells directly influences the efficacy of chemotherapy treatments. T cell activation takes place in the lymph node through T-cell receptor (TCR) recognition of MHC class I molecules, which activate CD8+ T cells, and MHC class II

molecules, which activate CD4+ T cells, expressed on mature dendritic cells. CD8+ cells and NK cells are some of the most cytotoxic cells involved in cancer cell lysis, and they secrete pro-inflammatory cytokines such as IL-2, IFN-γ, and TNF. These are also secreted by Th1 cells, which differentiate from naïve CD4+ T cells, and are important in the activation of macrophages, which can differentiate into two types: classically activated M1 macrophages and alternatively activated M2 macrophages. M1 macrophages contribute to the inflammatory response by releasing cytokines such as TNF and IL-12, while M2 macrophages contribute to wound repair and the anti-inflammatory response by releasing cytokines such as IL-10 and TGF-β and promote Th2 responses. Of note is that this M1/M2 dichotomy is a simplification, as macrophages exhibit high plasticity depending on their environmental signals [40]. However, we consider macrophage polarisation and repolarisation between these types to account for this simplification. We also consider Tregs, which mediate inflammatory processes such as reducing the synthesis of pro-inflammatory cytokines by producing immunosuppressive cytokines such as TGF-β and IL-10.

In this paper, we construct a mechanistic mathematical model of HGSOC using delay differential equations, incorporating immune cells, including CD4+ and CD8+ T cells, dendritic cells, macrophages, NK cells, cytokines, and damage-associated molecular patterns. We use experimental data to estimate the model's initial conditions and parameter values, incorporating deconvolution of bulk RNA-sequencing data from the TCGA OV database. Finally, we optimise the first-line neoadjuvant treatment of advanced HGSOC with carboplatin and paclitaxel, focusing on maximising efficacy, minimising toxicity, and improving treatment efficiency.

2 Mathematical Model of Ovarian Cancer

2.1 Modelling Assumptions

We assume cancer cell necrosis by tumour necrosis factor (TNF), interferon gamma (IFN-γ), and from the first-line chemotherapy treatment with paclitaxel. The necrosis of cancer cells releases danger-associated molecular patterns (DAMPs). In our model, we consider the DAMPs High Mobility Group Box 1 (HMGB1) and surface calreticulin, which bind to their respective receptors on immature dendritic cells (DCs), promoting their maturation and the presentation of tumour antigens [41]. Mature DCs migrate from the TS to the tumour-draining lymph node (TDLN) through chemokine circuits, where they prime naïve CD8+ T cells, CD4+ T cells and regulatory T cells (Tregs) [42, 43]. Upon DC activation, naïve CD8+ T cells undergo clonal expansion into mature cytotoxic CD8+ T cells in the TDLN [44]. We assume that naïve CD4+ T cells differentiate into either Th1 or Th2 T cells and then undergo clonal expansion in the TDLN. In the TLDN, naïve Tregs are activated by mature DCs and then undergo clonal expansion and proliferation. Chemotherapy inhibits the proliferation of all T cells in the TDLN, and after clonal expansion, these cells migrate to the TS. A diagram of these processes is provided in Figure 1.

We also examine seven key cytokines involved in the pathogenesis of ovarian cancer, as shown in Figure 2. The pro-inflammatory cytokines include interleukin-2 (IL-2), interleukin-12 (IL-12), interferon-γ (IFN-γ), and tumour necrosis factor (TNF). We assume IL-2 is primarily released by CD8+ T cells and Th1 T cells. It plays a crucial role as a growth factor for the proliferation of CD8+ T cells, Th1 T cells, and NK cells [45, 46]. IL-12, produced by dendritic cells and M1 macrophages, is key to the activation and proliferation of NK cells [47]. IFN-γ and TNF, produced by Th1 cells, NK cells, and CD8+ T cells, promote the polarisation of macrophages to the M1 pro-inflammatory phenotype and

induce the necrosis of cancer cells [48, 49].

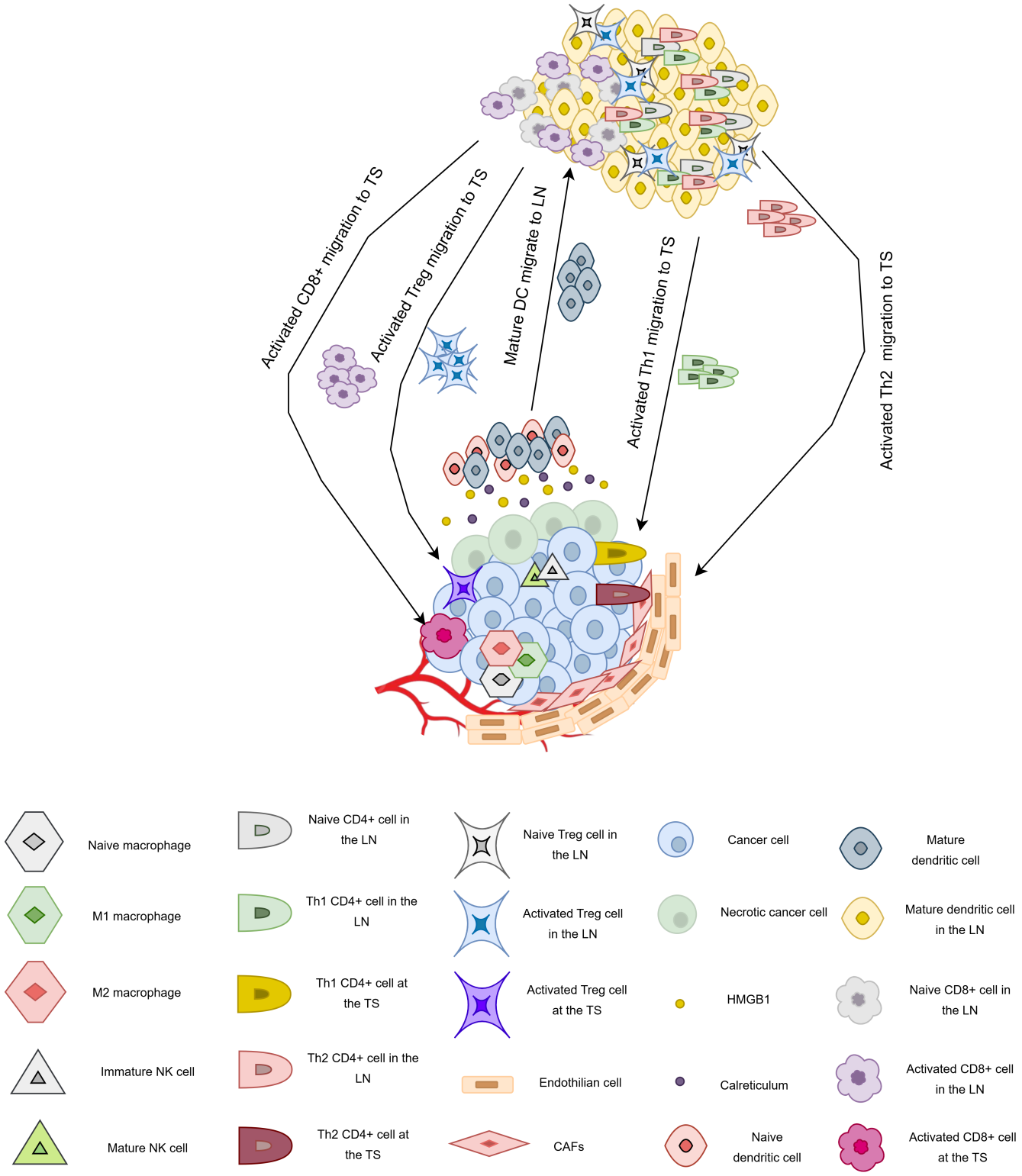

Figure 1: The relationship between the TS (bottom) and TLDN (top). DAMPs released by necrotic cancer cells activate a proportion of native DCs to mature and travel to the LN, with the cancer antigen, where they activate naïve CD8+, CD4+ T and Tregs. In the TDLN, these cells differentiate into effector CD8+ T cells, Th1, Th2 and Tregs, and upon maturation, migrate to the TS.

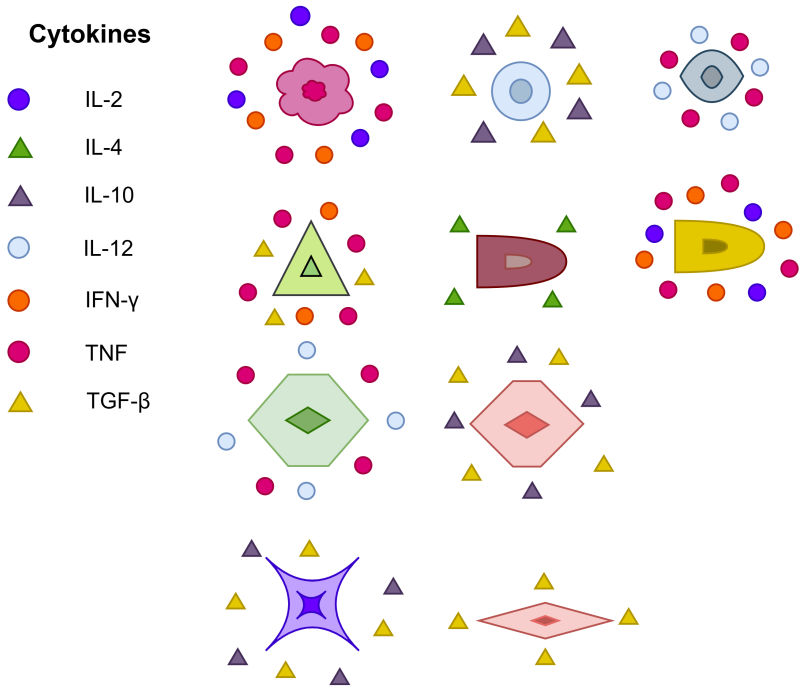

Figure 2: Immune cells and the cytokines they release. Pro-inflammatory cytokines are displayed by a circle, and anti-inflammatory cytokines are displayed by a triangle.

We also consider interleukin-4 (IL-4), interleukin-10 (IL-10), and transforming growth factor-β (TGF-β) as key anti-inflammatory cytokines. IL-4 and IL-10 promote the polarisation of naïve and M1 macrophages into the M2 type. We also assume, IL-4 is produced by Th2 cells, while IL-10 is produced by Tregs, M2 macrophages, and cancer cells. TGF-β, primarily involved in inhibiting CD8+ T cells and NK cells in cancer lysis, is produced by Tregs, cancer cells, M2 macrophages, and NK cells.

Additionally, we note that chemotherapy, including carboplatin and paclitaxel, works by killing rapidly proliferating cells, including cancer cells and T cells. In particular, carboplatin binds to DNA, interfering with DNA synthesis in the S phase of the cell cycle, inhibiting replication and leading to apoptosis [50, 51]. However, paclitaxel induces mitotic arrest at the G2/M phases of the cell cycle, disturbing cell division, and resulting in cell death [52, 53]. We model this by considering carboplatin and paclitaxel apoptosis and necrosis of cancer cells within the growth term, and by inhibiting CD8+ and CD4+ cell proliferation in the TDLN after activation.

We also assume the following biological and modelling conditions. Immature dendritic cells are cancer antigen-bearing and are activated by a proportion of DAMPs released by necrotic cells. This stimulates immature dendritic cells to mature and a proportion of these travel to the TDLN. When mature DCs in the TDLN activate naïve CD8+ and CD4+ T cells, the T cells differentiate and activate instantaneously, with their naïve cell concentrations remaining unchanged during proliferation. Effector and activated cells produce cytokines, and macrophages follow an M1/M2 dichotomy. A constant solution history is used, with each species' history set to its respective initial condition, and each component X degrades at a rate d_X, proportional to its concentration. All variables and their units are shown in Table 1.

Finally, we assume that the rate of activation and polarisation of X by Y follows the Michaelis-Menten kinetic law $\lambda_{XY}\frac{Y}{K_{XY}+Y}$, where λ_{XY} is the rate constant and K_{XY} is the half-saturation constant. We

Table 1: Variables used in the model, with variables in the top boxes having units of cell/cm^3, and all other variables having units of g/cm^3. All quantities refer to tumour site density/concentration unless otherwise specified. TDLN denotes the tumour-draining lymph node, whilst TS denotes the tumour site.

Var	Description	Var	Description
C	Viable cancer cell density	N	Necrotic cancer cell density
H	HMGB1	R	Calreticulin
D_0	Naïve dendritic cell density	D	Mature dendritic cell density
D_L	Mature dendritic cell density in the TDLN	T_0^8	Naïve CD8+ T cell density in the TDLN
T_8	Effector CD8+ T cell density in the TDLN	T_8	CD8+ T cell density in the TS
T_0^4	Naïve CD4+ T cell density in the TDLN	L_1	Effector Th1 cell density in the TDLN
T_1	Effector Th1 cell density in the TS	L_2	Effector Th2 cell density in the TDLN
T_2	Effector Th2 cell density in the TS	L_0^r	Naïve Treg cell density in the TDLN
L_r	Effector Treg cell density in the TDLN	T_r	Effector Treg cell density in the TS
M_0	Naïve macrophages	M_1	M1 macrophage density
M_2	M2 macrophage density	K_0	Naïve NK cell density
K	Activated NK cell density	I_2	IL-2 concentration
I_4	IL-4 concentration	I_{12}	IL-12 concentration
I_{10}	IL-10 concentration	I_γ	IFN-γ concentration
I_α	TNF concentration	I_β	TGF-β concentration
P	Paclitaxel concentration in the TS	A	Carboplatin concentration in the TS
P^{LN}	Paclitaxel concentration in the TDLN	A^{LN}	Carboplatin concentration in the TDLN

model the rate of inhibition of X by Y using $\frac{1}{1+Y/K_{XY}}$, where λ_{XY} is the rate constant and K_{XY} is the half-saturation constant. We model the production of X by Y using mass-action kinetics using $\lambda_{XY}XY$ for some positive constant λ_{XY}. We also assume that lysis of X by Y follows mass-action when Y is a cell, and Michaelis-Menten when Y is a cytokine.

2.2 Model Equations

The model equations and structure follow similarly to many of the model equations in [36] and [37].

2.2.1 Equation for Cancer Cells (C)

The first term models cancer growth using a logistic function, where r_C is the baseline growth rate and C_0 is the carrying capacity. It also accounts for apoptosis induced by paclitaxel and carboplatin, with paclitaxel additionally inducing immunogenic cell death. The second term accounts for CD8+ T cell lysis of the cancer cells, with this process inhibited by TGF-β [54, 55]. The third and fourth terms model CD4+ Th1 and NK cell recognition and lysis of cancer cells, respectively [56–58]. Tregs also inhibit the cytotoxicity of CD8+ T cells, CD4+ T cells and NK cells, and are accounted for in the second, third and fourth terms [59–61]. TGF-β also inhibits the cytotoxicity of NK cells, as shown in the fourth term [62]. Lastly, the fifth and sixth terms model cancer cell necroptosis by TNF [63, 64]

and IFN-γ [65]. This gives us

$$\begin{aligned}\frac{dC}{dt} = r_C \underbrace{C\left(1-\frac{C}{C_0}\right)}_{\text{growth}} \underbrace{\left(1-\lambda_{CP}\frac{P}{K_{CP}+P}-\nu_{CP}\frac{P}{K_{CP}+P}-\lambda_{CA}\frac{A}{K_{CA}+A}\right)}_{\substack{\text{apoptosis by } P,\ A,\\ \text{necrosis by } P}} \\ \underbrace{-\lambda_{CT_8}T_8C\left(\frac{1}{1+I_\beta/K_{T_8I_\beta}}\right)\left(\frac{1}{1+T_r/K_{T_8T_r}}\right)}_{\substack{\text{lysis by } T_8\\ \text{inhibited by } I_\beta \text{ and } T_r}} \\ \underbrace{-\lambda_{CT_1}T_1C\left(\frac{1}{1+T_r/K_{T_1T_r}}\right)}_{\substack{\text{lysis by } T_1\\ \text{inhibited by } T_r}} \underbrace{-\lambda_{CK}KC\left(\frac{1}{1+I_\beta/K_{KI_\beta}}\right)\left(\frac{1}{1+T_r/K_{KT_r}}\right)}_{\substack{\text{lysis by } K\\ \text{inhibited by } I_\beta \text{ and } T_r}} \\ \underbrace{-\lambda_{CI_\alpha}C\left(\frac{I_\alpha}{K_{CI_\alpha}+I_\alpha}\right)}_{\text{elimination by } I_\alpha} \underbrace{-\lambda_{CI_\gamma}C\left(\frac{I_\gamma}{K_{CI_\gamma}+I_\gamma}\right)}_{\text{elimination by } I_\gamma}.\end{aligned} \tag{2.1}$$

2.2.2 Equation for Necrotic Cells (N)

The first to third terms account for cancer cell necrosis by TNF, IFN-γ and paclitaxel, respectively [63–65]. This gives us

$$\begin{aligned}\frac{dN}{dt} = \underbrace{\lambda_{CI_\alpha}C\left(\frac{I_\alpha}{K_{CI_\alpha}+I_\alpha}\right)}_{\text{elimination by } I_\alpha} + \underbrace{\lambda_{CI_\gamma}C\left(\frac{I_\gamma}{K_{CI_\gamma}+I_\gamma}\right)}_{\text{elimination by } I_\gamma} + \\ \underbrace{r_CC\left(1-\frac{C}{C_0}\right)}_{\text{growth}}\underbrace{\nu_{CP}\frac{P}{K_{CP}+P}}_{\text{necrosis by } P} - \underbrace{d_NN}_{\text{removal}}.\end{aligned} \tag{2.2}$$

2.2.3 Equation for HMGB1 (H)

As shown in the first term, we assume that a proportion of necrotic cells release HMGB1 [66] This gives us

$$\frac{dH}{dt} = \underbrace{\lambda_{NH}N}_{\text{HMGB1 release by } N} - \underbrace{d_HH}_{\text{degradation}}. \tag{2.3}$$

2.2.4 Equation for Calreticulin (R)

As shown in the first term, we assume that a proportion of necrotic cells release calreticulin [66]. This gives us

$$\frac{dR}{dt} = \underbrace{\lambda_{NR}N}_{\text{Calreticulin release by } N} - \underbrace{d_RR}_{\text{degradation}}. \tag{2.4}$$

2.2.5 Equation for Immature DCs in the TS (D_0)

In the first term, we assume that immature dendritic cells are supplied at a constant rate $\mathcal{A}_{D_0}$. In the second term, DAMPs activate a proportion of DCs in the TS, with DC maturation in the TS inhibited by IL-10 and TGF-β [67, 68]. This gives us

$$\frac{dD_0}{dt} = \underbrace{\mathcal{A}_{D_0}}_{D_0 \text{ supply}} - \left(\underbrace{\zeta_{DH} D_0 \frac{H}{K_{DH} + H}}_{D_0 \to D \text{ by } H} + \underbrace{\zeta_{DR} D_0 \frac{R}{K_{DR} + R}}_{D_0 \to D \text{ by } R} \right) \times \underbrace{\frac{1}{1 + I_{10}/K_{DI_{10}}}}_{\text{inhibition by } I_{10}} \times \underbrace{\frac{1}{1 + I_\beta/K_{DI_\beta}}}_{\text{inhibition by } I_\beta} - \underbrace{d_{D_0} D_0}_{\text{degradation}} . \tag{2.5}$$

2.2.6 Equation for Mature DCs in the TS (D)

The first term accounts for the activation of DCs from (2.5) and the second term assumes that a proportion of mature DCs migrate to the TDLN. This gives us

$$\frac{dD}{dt} = \left(\underbrace{\zeta_{DH} D_0 \frac{H}{K_{DH} + H}}_{D_0 \to D \text{ by } H} + \underbrace{\zeta_{DR} D_0 \frac{R}{K_{DR} + R}}_{D_0 \to D \text{ by } R} \right) \times \underbrace{\frac{1}{1 + I_{10}/K_{DI_{10}}}}_{\text{inhibition by } I_{10}} \times \underbrace{\frac{1}{1 + I_\beta/K_{DI_\beta}}}_{\text{inhibition by } I_\beta} - \underbrace{\lambda_{D_L D} D}_{\substack{\text{migration to} \\ \text{the TDLN}}} - \underbrace{d_D D}_{\text{degradation}} . \tag{2.6}$$

2.2.7 Equation for Mature DCs in the TDLN (D_L)

The exponential in the first term accounts for the degradation of DCs during the transit, of time τ_m, from the TS to the TDLN. The degradation rate during transit is similar to the degradation of mature dendritic cells in the TS, and we assume that they are the same [69]. As the volume between the TS and TDLN is different, we account for the volume change to maintain the correct concentrations by multiplying by $V_{\text{TS}}/V_{\text{LN}}$, where V_{TS} is the volume of the TS, and V_{LN} is the volume of the LN. We also consider the transit time of dendritic cells arriving at the TDLN as having left the TS at time $t - \tau_m$. This gives us

$$\frac{dD_L}{dt} = \underbrace{\frac{V_{\text{TS}}}{V_{\text{LN}}} e^{-d_D \tau_m} \lambda_{D_L D} D(t - \tau_m)}_{\text{migration to the TDLN}} - \underbrace{d_{D_L} D_L}_{\text{degradation}} . \tag{2.7}$$

2.2.8 Equation for Naïve CD8+ T Cells in the TDLN (T_0^8)

We assume that naïve CD8+ T cells are supplied at a rate $\mathcal{A}_{T_0^8}$ in the first term. The second term accounts for the activation of naïve CD8+ T cells by DCs in the TDLN, inhibited by Tregs [70, 71]. We assume that this activation is instant, and gives us

$$\frac{dT_0^8}{dt} = \underbrace{\mathcal{A}_{T_0^8}}_{\text{source}} - \underbrace{\zeta_{L_8 D_L} T_0^8 D_L}_{T_0^8 \to L_8 \text{ by } D_L} \times \underbrace{\frac{1}{1 + L_r/K_{T_0^8 L_r}}}_{\text{inhibition by } L_r} - \underbrace{d_{T_0^8} T_0^8}_{\text{degradation}} . \tag{2.8}$$

2.2.9 Equation for Effector CD8+ T Cells in the TDLN (L_8)

The exponential in the first term accounts for the degradation of activated CD8+ T cells during proliferation dependent on τ_8, the time for T_8 to complete clonal expansion, and N_8, the number of cell divisions in clonal expansion before proliferation stops. We assume proliferation takes τ_8 time to finish, the degradation rate during proliferation is the same for effector CD8+ T cells in the TDLN, and that the concentration of effector Tregs in the TDLN does not change significantly during proliferation. We also consider the activation of T_0^8 by D_L at time $t-\tau_8$, and the inhibition of CD8+ T cell proliferation due to Tregs, carboplatin and paclitaxel [51, 52, 72].

In particular, since the killing of proliferating CD8+ T cells in the TDLN due to carboplatin and paclitaxel occurs during the whole proliferation process, it is not sufficient to consider point estimates of carboplatin and paclitaxel concentration. Instead, we resort to considering the integrals of the concentrations of the relevant species throughout the entire τ_8 time that it takes for the cell division program to be completed. This is because these integrals are proportional (with a proportionality constant of $1/\tau_8$) to the average concentration of these species throughout activation, allowing us to properly incorporate the inhibition.

The second term accounts for the migration of effector CD8+ T cells from the TDLN to the TS. This gives us

$$\frac{dL_8}{dt} = \underbrace{\frac{e^{-d_{L_8}\tau_8} 2^{N_8} \zeta_{L_8 D_L} T_0^8(t-\tau_8) D_L(t-\tau_8)}{\left(1+\int_{t-\tau_8}^{t} P^{\mathrm{LN}}(s)\, ds/K_{L_8 P^{\mathrm{LN}}}\right)\left(1+\int_{t-\tau_8}^{t} A^{\mathrm{LN}}(s)\, ds/K_{L_8 A^{\mathrm{LN}}}\right)(1+L_r(t-\tau_8)/K_{L_8 L_r})}}_{\text{proliferation of } L_8\text{, inhibited by } P^{\mathrm{LN}},\ A^{\mathrm{LN}} \text{ and } L_r} - \underbrace{\zeta_{T_8 L_8} L_8}_{\text{migration to TS}} - \underbrace{d_{L_8} L_8}_{\text{degradation}} . \tag{2.9}$$

2.2.10 Equation for Effector CD8+ T Cells in the TS (T_8)

The exponential in the first term accounts for the degradation of effector CD8+ T cells during the transit of time τ_a from the TS to the TDLN. We account for the volume difference between the TDLN and TS by multiplying this term by $V_{\mathrm{LN}}/V_{\mathrm{TS}}$. We further assume that the degradation during transit is the same as the degradation of effector CD8+ T cells in the TS, and consider the transit time of DCs arriving in the TS as having left the TDLN at time $t-\tau_a$. The second term accounts for the proliferation of CD8+ T cells in the TS by IL-2, inhibited by Tregs [71, 73]. The third term accounts for the degradation of CD8+ T cells in the TS, inhibited by IL-10 [74]. Thus,

$$\frac{dT_8}{dt} = \underbrace{\frac{V_{\mathrm{LN}}}{V_{\mathrm{TS}}} e^{-d_{L_8}\tau_a} \zeta_{T_8 L_8} L_8(t-\tau_a)}_{\text{migration to TS}} + \left(\underbrace{\lambda_{T_8 I_2} T_8 \frac{I_2}{K_{T_8 I_2} + I_2}}_{\text{proliferation by } I_2}\right) \times \underbrace{\frac{1}{1+T_r/K_{T_8 T_r}}}_{\text{inhibition by } T_r} - \underbrace{\frac{d_{T_8} T_8}{1+I_{10}/K_{T_8 I_{10}}}}_{\substack{\text{degradation}\\ \text{inhibited by } I_{10}}} . \tag{2.10}$$

2.2.11 Equation for Naïve CD4+ T Cells in the TDLN (T_0^4)

In the first term, we assume that naïve CD4+ T cells are supplied at a rate $\mathcal{A}_{T_0^4}$. In the second term, we account for DC-induced activation of naïve CD4+ T cells which differentiate into the Th1 and Th2

phenotypes, respectively, in the TDLN inhibited by Tregs [70, 71]. This gives us that

$$\frac{dT_0^4}{dt} = \underbrace{\mathcal{A}_{T_0^4}}_{\text{source}} - \left(\underbrace{\zeta_{L_1 D_L} T_0^4 D_L}_{T_0^4 \to L_1 \text{ by } D_L} + \underbrace{\zeta_{L_2 D_L} T_0^4 D_L}_{T_0^4 \to L_2 \text{ by } D_L} \right) \times \underbrace{\frac{1}{1 + L_r / K_{T_0^4 L_r}}}_{\text{inhibition by } L_r} - \underbrace{d_{T_0^4} T_0^4}_{\text{degradation}} . \tag{2.11}$$

2.2.12 Equation for Effector Th1 Cells in the TDLN (L_1)

The exponential in the first term accounts for the degradation of activated Th1 cells during proliferation dependent on τ_1, the time for L_1 to complete clonal expansion, and N_1, the number of cell divisions in clonal expansion before proliferation stops. We assume that proliferation takes τ_1 time to finish, the degradation during proliferation is the same as the degradation of effector Th1 cells in the TDLN, and that the concentration of effector Tregs in the TDLN does not change significantly during proliferation. We also consider the activation of T_0^4 to L_1 by D_L at time $t - \tau_1$, and the inhibition of Th1 cell proliferation due to carboplatin, paclitaxel and Tregs [72]. The second term accounts for the migration of effector Th1 cells from the TDLN to the TS. This gives us

$$\begin{aligned} \frac{dL_1}{dt} = & \underbrace{\frac{e^{-d_{L_1}\tau_1} 2^{N_1} \zeta_{L_1 D_L} T_0^4(t-\tau_1) D_L(t-\tau_1)}{\left(1 + \int_{t-\tau_1}^{t} P^{\text{LN}}(s)\, ds / K_{L_1 P^{\text{LN}}}\right) \left(1 + \int_{t-\tau_1}^{t} A^{\text{LN}}(s)\, ds / K_{L_1 A^{\text{LN}}}\right) (1 + L_r(t-\tau_1)/K_{L_1 L_r})}}_{\text{proliferation of } L_1\text{, inhibited by } P^{\text{LN}},\ A^{\text{LN}} \text{ and } L_r} \\ & - \underbrace{\zeta_{T_1 L_1} L_1}_{\text{migration to TS}} - \underbrace{d_{L_1} L_1}_{\text{degradation}} . \end{aligned} \tag{2.12}$$

2.2.13 Equation for Effector Th1 Cells in the TS (T_1)

The exponential in the first term accounts for the degradation of effector Th1 cells during the transit of time τ_b from the TS to the TDLN. We account for the volume difference between the TDLN and TS by multiplying this term by $V_{\text{LN}}/V_{\text{TS}}$ and consider the transit time of DCs arriving in the TS as having left the TDLN at time $t - \tau_b$. We assume that the degradation rate during transit is the same as the degradation of effector Th1 cells in the TS. The second term accounts for the proliferation of effector Th1 cells in the TS by IL-2 [75]. This gives us

$$\frac{dT_1}{dt} = \underbrace{\frac{V_{\text{LN}}}{V_{\text{TS}}} e^{-d_{L_1}\tau_b} \zeta_{T_1 L_1} L_1(t-\tau_b)}_{\text{migration to TS}} + \underbrace{\lambda_{T_1 I_2} T_1 \frac{I_2}{K_{T_1 I_2} + I_2}}_{\text{proliferation by } I_2} - \underbrace{d_{T_1} T_1}_{\text{degradation}} . \tag{2.13}$$

2.2.14 Equation for Effector Th2 Cells in the TDLN (L_2)

The exponential in the first term accounts for the degradation of activated Th2 cells during proliferation dependent on τ_2, the time for L_2 to complete clonal expansion, and N_2, the number of cell divisions in clonal expansion before proliferation stops. We assume that proliferation takes τ_2 time to finish, and that the degradation during proliferation is the same as the degradation of effector Th2 cells in the TDLN. We also consider the activation of T_0^4 to L_2 by D_L at time $t - \tau_2$, and the inhibition of Th2 cell proliferation due to carboplatin and paclitaxel. The second term accounts for the migration

of effector Th2 cells from the TDLN to the TS. This gives us

$$\frac{dL_2}{dt} = \underbrace{\frac{e^{-d_{L_2}\tau_2} 2^{N_2} \zeta_{L_2 D_L} T_0^4(t-\tau_2) D_L(t-\tau_2)}{\left(1+\int_{t-\tau_2}^{t} P^{\mathrm{LN}}(s)\ ds/K_{L_2 P^{\mathrm{LN}}}\right)\left(1+\int_{t-\tau_2}^{t} A^{\mathrm{LN}}(s)\ ds/K_{L_2 A^{\mathrm{LN}}}\right)}}_{\text{proliferation of } L_2\text{, inhibited by } P^{\mathrm{LN}} \text{ and } A^{\mathrm{LN}}} - \underbrace{\zeta_{T_2 L_2} L_2}_{\text{migration to TS}} - \underbrace{d_{L_2} L_2}_{\text{degradation}} . \tag{2.14}$$

2.2.15 Equation for Effector Th2 Cells in the TS (T_2)

The exponential in the first term accounts for the degradation of activated Th2 cells during the transit of time τ_c from the TS to the TDLN. We account for the volume difference between the TDLN and TS by multiplying this term by $V_{\mathrm{LN}}/V_{\mathrm{TS}}$. We also consider the transit time of DCs arriving in the TS as having left the TDLN at time $t-\tau_c$. We assume that the degradation during transit is the same as the degradation of effector Th2 cells in the TS. The second term accounts for the proliferation of effector Th2 cells in the TS by IL-4 [76]. Finally, This gives us

$$\frac{dT_2}{dt} = \left(\underbrace{\frac{V_{\mathrm{LN}}}{V_{\mathrm{TS}}} e^{-d_{T_2}\tau_c} \zeta_{T_2 L_2} L_2(t-\tau_c)}_{\text{migration to TS}}\right) + \underbrace{\lambda_{T_2 I_4} T_2 \frac{I_4}{K_{T_2 I_4} + I_4}}_{\text{proliferation by } I_4} - \underbrace{d_{T_2} T_2}_{\text{degradation}} . \tag{2.15}$$

2.2.16 Equation for Naïve Tregs in the TDLN (L_0^r)

In the first term, we assume that naïve Tregs come from a source $\mathcal{A}_T$ mainly from the thymus [77]. The second term accounts for the activation of L_0^r by D_L. This gives us

$$\frac{dL_0^r}{dt} = \underbrace{\mathcal{A}_T}_{\text{source}} - \underbrace{\zeta_{L_r D_L} L_0^r D_L}_{L_0^r \to L_r \text{ by } D_L} - \underbrace{d_{L_0^r} L_0^r}_{\text{degradation}} . \tag{2.16}$$

2.2.17 Equation for Effector Tregs in the TDLN (L_r)

The exponential in the first term accounts for the degradation of activated Tregs during proliferation dependent on τ_r, the time for L_r to complete clonal expansion, and N_r, the number of cell divisions in clonal expansion before proliferation stops. We assume that proliferation occurs with a delay of τ_r after activation, and that the degradation during proliferation is the same as the degradation of effector Tregs in the TDLN. We also consider the activation of T_0^r to L_r by D_L at time $t-\tau_r$, and the inhibition of Treg cell proliferation due to carboplatin and paclitaxel. The second term accounts for the migration of Tregs from the TDLN to the TS. This gives us

$$\frac{dL_r}{dt} = \underbrace{\frac{e^{-d_{L_r}\tau_r} 2^{N_r} \zeta_{L_r D_L} L_0^r(t-\tau_r) D_L(t-\tau_r)}{\left(1+\int_{t-\tau_r}^{t} P^{\mathrm{LN}}(s)\ ds/K_{L_r P^{\mathrm{LN}}}\right)\left(1+\int_{t-\tau_r}^{t} A^{\mathrm{LN}}(s)\ ds/K_{L_r A^{\mathrm{LN}}}\right)}}_{\text{proliferation of } L_r\text{, inhibited by } P^{\mathrm{LN}} \text{ and } A^{\mathrm{LN}}} - \underbrace{\zeta_{T_r L_r} L_r}_{\text{migration to TS}} - \underbrace{d_{L_r} L_r}_{\text{degradation}} . \tag{2.17}$$

2.2.18 Equation for Effector Tregs in the TS (T_r)

The exponential in the first term accounts for the degradation of effector Tregs during the transit of time τ_d from the TS to the TDLN. We account for the volume difference between the TDLN and TS

by multiplying this term by $V_{\text{LN}}/V_{\text{TS}}$. We assume that the degradation during transit is the same as the degradation of effector Tregs in the TS. We also consider the transit time of dendritic cells arriving in the TS as having left the TDLN at time $t - \tau_d$. The second term accounts for the proliferation of effector Tregs in the TS by TGF-β [78]. This gives us

$$\frac{dT_r}{dt} = \underbrace{\frac{V_{\text{LN}}}{V_{\text{TS}}} e^{-d_{T_r}\tau_d} \zeta_{T_r L_r} L_r(t-\tau_d)}_{\text{migration to TS}} + \underbrace{\lambda_{T_r I_\beta} T_r \frac{I_\beta}{K_{T_r I_\beta} + I_\beta}}_{\text{proliferation by } I_\beta} - \underbrace{d_{T_r} T_r}_{\text{degradation}} . \tag{2.18}$$

2.2.19 Equations for Naïve (M_0), M1 (M_1) and M2 (M_2) Macrophages

In the first term, we assume that naïve macrophages are supplied at a rate $\mathcal{A}_{M_0}$. The second and third terms account for IFN-γ and TNF stimulating the polarisation of naïve macrophages toward the pro-inflammatory M1 phenotype, respectively, and the fourth and fifth terms account for IL-4 and IL-10 stimulating the polarisation of naïve macrophages toward the anti-inflammatory M2 phenotype [79–81]. This gives us

$$\begin{aligned}\frac{dM_0}{dt} = {} & \underbrace{\mathcal{A}_{M_0}}_{\text{source}} - \underbrace{\zeta_{M_1 I_\gamma} M_0 \frac{I_\gamma}{K_{M_1 I_\gamma} + I_\gamma}}_{M_0 \to M_1 \text{ by } I_\gamma} - \underbrace{\zeta_{M_1 I_\alpha} M_0 \frac{I_\alpha}{K_{M_1 I_\alpha} + I_\alpha}}_{M_0 \to M_1 \text{ by } I_\alpha} \\ & - \underbrace{\zeta_{M_2 I_4} M_0 \frac{I_4}{K_{M_2 I_4} + I_4}}_{M_0 \to M_2 \text{ by } I_4} - \underbrace{\zeta_{M_2 I_{10}} M_0 \frac{I_{10}}{K_{M_2 I_{10}} + I_{10}}}_{M_0 \to M_2 \text{ by } I_{10}} - \underbrace{d_{M_0} M_0}_{\text{degradation}} .\end{aligned} \tag{2.19}$$

The first and second terms account for IFN-γ and TNF stimulating the polarisation of naïve macrophages toward the pro-inflammatory M1 phenotype from (2.19). The third and fourth terms account for IFN-γ and TNF stimulating the re-polarisation of M2 macrophages toward the pro-inflammatory M1 phenotype, and the fifth term accounts for TGF-β stimulating the re-polarisation of M1 macrophages toward the M2 anti-inflammatory phenotype [82–84]. This gives us

$$\begin{aligned}\frac{dM_1}{dt} = {} & \underbrace{\zeta_{M_1 I_\gamma} M_0 \frac{I_\gamma}{K_{M_1 I_\gamma} + I_\gamma}}_{M_0 \to M_1 \text{ by } I_\gamma} + \underbrace{\zeta_{M_1 I_\alpha} M_0 \frac{I_\alpha}{K_{M_1 I_\alpha} + I_\alpha}}_{M_0 \to M_1 \text{ by } I_\alpha} + \underbrace{\zeta_{M I_\gamma} M_2 \frac{I_\gamma}{K_{M_1 I_\gamma} + I_\gamma}}_{M_2 \to M_1 \text{ by } I_\gamma} \\ & + \underbrace{\zeta_{M I_\alpha} M_2 \frac{I_\alpha}{K_{M_1 I_\alpha} + I_\alpha}}_{M_2 \to M_1 \text{ by } I_\alpha} - \underbrace{\zeta_{M I_\beta} M_1 \frac{I_\beta}{K_{M_2 I_\beta} + I_\beta}}_{M_1 \to M_2 \text{ by } I_\beta} - \underbrace{d_{M_1} M_1}_{\text{degradation}} .\end{aligned} \tag{2.20}$$

The first and second terms account for IL-4 and IL-10 stimulating the polarisation of naïve macrophages toward the anti-inflammatory M2 phenotype from (2.19). The third and fourth terms account for IFN-γ and TNF stimulating the re-polarisation of M2 macrophages toward the pro-inflammatory M1 phenotype from (2.20). The fifth term accounts for TGF-β re-polarisation of M1 macrophages toward the anti-inflammatory M2 phenotype from (2.20). This gives us

$$\begin{aligned}\frac{dM_2}{dt} = {} & \underbrace{\zeta_{M_2 I_4} M_0 \frac{I_4}{K_{M_2 I_4} + I_4}}_{M_0 \to M_2 \text{ by } I_4} + \underbrace{\zeta_{M_2 I_{10}} M_0 \frac{I_{10}}{K_{M_2 I_{10}} + I_{10}}}_{M_0 \to M_2 \text{ by } I_{10}} - \underbrace{\zeta_{M I_\gamma} M_2 \frac{I_\gamma}{K_{M_1 I_\gamma} + I_\gamma}}_{M_2 \to M_1 \text{ by } I_\gamma} \\ & - \underbrace{\zeta_{M I_\alpha} M_2 \frac{I_\alpha}{K_{M_1 I_\alpha} + I_\alpha}}_{M_2 \to M_1 \text{ by } I_\alpha} + \underbrace{\zeta_{M I_\beta} M_1 \frac{I_\beta}{K_{M_2 I_\beta} + I_\beta}}_{M_1 \to M_2 \text{ by } I_\beta} - \underbrace{d_{M_2} M_2}_{\text{degradation}} .\end{aligned} \tag{2.21}$$

2.2.20 Equations for Naïve (K_0) and Activated (K) NK cells

In the first term, we assume naïve NK cells are supplied at a rate $\mathcal{A}_{K_0}$. The second and third terms account for NK cell activation by IL-2 and IL-12, respectively [85, 86]. This gives us

$$\frac{dK_0}{dt} = \underbrace{\mathcal{A}_{K_0}}_{\text{source}} - \underbrace{\zeta_{KI_2} K_0 \frac{I_2}{K_{KI_2} + I_2}}_{K_0 \to K \text{ by } I_2} - \underbrace{\zeta_{KI_{12}} K_0 \frac{I_{12}}{K_{KI_{12}} + I_{12}}}_{K_0 \to K \text{ by } I_{12}} - \underbrace{d_{K_0} K_0}_{\text{degradation}} . \tag{2.22}$$

The first and second terms account for NK cell activation by IL-2 and IL-12 from (2.22). IL-2 [85] and IL-12 [87] also promote NK cell proliferation, shown in the third and fourth terms, respectively. This gives us

$$\frac{dK}{dt} = \underbrace{\zeta_{KI_2} K_0 \frac{I_2}{K_{KI_2} + I_2}}_{K_0 \to K \text{ by } I_2} + \underbrace{\zeta_{KI_{12}} K_0 \frac{I_{12}}{K_{KI_{12}} + I_{12}}}_{K_0 \to K \text{ by } I_{12}} + \underbrace{\lambda_{KI_2} K \frac{I_2}{K_{KI_2} + I_2}}_{\text{proliferation by } I_2} + \underbrace{\lambda_{KI_{12}} K \frac{I_{12}}{K_{KI_{12}} + I_{12}}}_{\text{proliferation by } I_{12}} - \underbrace{d_K K}_{\text{degradation}} . \tag{2.23}$$

2.2.21 Equation for IL-2 (I_2)

The equation accounts for IL-2 production by CD4+ Th1 and CD8+ T cells inhibited by Tregs [88, 89]. This gives us

$$\frac{dI_2}{dt} = \left(\underbrace{\lambda_{I_2T_1} T_1}_{\text{production by } T_1} + \underbrace{\lambda_{I_2T_8} T_8}_{\text{production by } T_8} \right) \times \underbrace{\frac{1}{1 + T_r/K_{I_2T_r}}}_{\text{inhibition by } T_r} - \underbrace{d_{I_2} I_2}_{\text{degradation}} . \tag{2.24}$$

2.2.22 Equation for IL-4 (I_4)

The equation accounts for the release of IL-4 by Th2 CD4+ T cells [80]. This gives us

$$\frac{dI_4}{dt} = \underbrace{\lambda_{I_4T_2} T_2}_{\text{production by } T_2} - \underbrace{d_{I_4} I_4}_{\text{degradation}} . \tag{2.25}$$

2.2.23 Equation for IL-10 (I_{10})

The first to third terms account for IL-10 production by Tregs, M2 macrophages and cancer cells, respectively [80, 90–92]. This gives us

$$\frac{dI_{10}}{dt} = \underbrace{\lambda_{I_{10}T_r} T_r}_{\text{production by } T_r} + \underbrace{\lambda_{I_{10}M_2} M_2}_{\text{production by } M_2} + \underbrace{\lambda_{I_{10}C} C}_{\text{production by } C} - \underbrace{d_{I_{10}} I_{10}}_{\text{degradation}} . \tag{2.26}$$

2.2.24 Equation for IL-12 (I_{12})

The first and second terms account for IL-12 production by mature DCs and activated M1 macrophages [93–95], respectively. This gives us

$$\frac{dI_{12}}{dt} = \underbrace{\lambda_{I_{12}D} D}_{\text{production by } D} + \underbrace{\lambda_{I_{12}M_1} M_1}_{\text{production by } M_1} - \underbrace{d_{I_{12}} I_{12}}_{\text{degradation}} . \tag{2.27}$$

2.2.25 Equation for IFN-γ (I_γ)

The first term accounts for IFN-γ production by CD4+ Th1 and NK cells inhibited by Tregs [80, 87, 96–98]. The second term accounts for IFN-γ production by CD8+ T cells [99]. This gives us

$$\frac{dI_\gamma}{dt} = \underbrace{\left(\lambda_{I_\gamma T_1} T_1 + \lambda_{I_\gamma K} K\right) \frac{1}{1 + T_r/K_{I_\gamma T_r}}}_{\substack{\text{production by } T_1 \text{ and K} \\ \text{inhibited by } T_r}} + \underbrace{\lambda_{I_\gamma T_8} T_8}_{\text{production by } T_8} - \underbrace{d_{I_\gamma} I_\gamma}_{\text{degradation}} . \tag{2.28}$$

2.2.26 Equation for TNF (I_α)

The first to fifth terms account for TNF production by CD8+ T cells, CD4+ Th1 cells, NK cells, M1 polarised macrophages and mature DCs [82, 94, 96, 99–101], respectively. This gives us

$$\frac{dI_\alpha}{dt} = \underbrace{\lambda_{I_\alpha T_8} T_8}_{\text{production by } T_8} + \underbrace{\lambda_{I_\alpha T_1} T_1}_{\text{production by } T_1} + \underbrace{\lambda_{I_\alpha K} K}_{\text{production by } K} + \underbrace{\lambda_{I_\alpha M_1} M_1}_{\text{production by } M_1} + \underbrace{\lambda_{I_\alpha D} D}_{\text{production by } D} - \underbrace{d_{I_\alpha} I_\alpha}_{\text{degradation}} . \tag{2.29}$$

2.2.27 Equation for TGF-β (I_β)

The first to fourth terms account for TGF-β production by Tregs, cancer cells, M2 polarised macrophages and NK cells, respectively [87, 102–105]. This gives us

$$\frac{dI_\beta}{dt} = \underbrace{\lambda_{I_\beta T_r} T_r}_{\text{production by } T_r} + \underbrace{\lambda_{I_\beta C} C}_{\text{production by } C} + \underbrace{\lambda_{I_\beta M_2} M_2}_{\text{production by } M_2} + \underbrace{\lambda_{I_\beta K} K}_{\text{production by } K} - \underbrace{d_{I_\beta} I_\beta}_{\text{degradation}} . \tag{2.30}$$

2.2.28 Equations for Paclitaxel (P and P^{LN})

We assume that paclitaxel is administered at a constant rate over a duration Δ_P intravenously at times $t_1^P, t_2^P, \ldots, t_n^P$ with doses $\xi_1^P, \xi_2^P, \ldots, \xi_n^P$ respectively. We account for the systemic nature of paclitaxel distribution and depletion due to killing cancer cells in the TS and killing CD8+ T cells, Th1 and Th2 cells, and Tregs in the TDLN. It is important to note that the administered dose is not equal to the corresponding change in concentration in the TS or the TDLN. For simplicity, we assume linear pharmacokinetics so that, for some scaling factor f_P, we have that

$$\frac{dP}{dt} = \underbrace{\sum_{j=1}^{n} \xi_j^P f_P \frac{\theta\left(t - t_j\right) - \theta\left(t - t_j - \Delta_P\right)}{\Delta_P}}_{\text{infusion}} - \underbrace{d_{PC} P C}_{\text{depletion due to killing } C} - \underbrace{d_P P}_{\text{degradation}} , \tag{2.31}$$

$$\begin{aligned} \frac{dP^{\text{LN}}}{dt} = & \underbrace{\sum_{j=1}^{n} \xi_j^P \frac{\theta\left(t - t_j\right) - \theta\left(t - t_j - \Delta_P\right)}{\Delta_P}}_{\text{infusion}} - \underbrace{d_{P^{\text{LN}} L_8} P^{\text{LN}} L_8}_{\text{depletion due to killing } L_8} - \underbrace{d_{P^{\text{LN}} L_1} P^{\text{LN}} L_1}_{\text{depletion due to killing } L_1} \\ & - \underbrace{d_{P^{\text{LN}} L_2} P^{\text{LN}} L_2}_{\text{depletion due to killing } L_2} - \underbrace{d_{P^{\text{LN}} L_r} P^{\text{LN}} L_r}_{\text{depletion due to killing } L_r} - \underbrace{d_P P^{\text{LN}}}_{\text{degradation}} . \end{aligned} \tag{2.32}$$

where $\theta(t)$ is the Heaviside function which equals 1 if $t \geq 0$, and 0 otherwise.

2.2.29 Equations for Carboplatin (A and A^{LN})

We assume that carboplatin is administered at a constant rate over a duration Δ_A intravenously at times $t_1^A, t_2^A, \ldots, t_n^A$ with doses $\xi_1^A, \xi_2^A, \ldots, \xi_n^A$ respectively. We account for the systemic nature of carboplatin distribution and depletion due to killing cancer cells in the TS and due to killing CD8+ T cells, Th1 and Th2 cells, and Tregs in the TDLN. It is important to note that the administered dose is not equal to the corresponding change in concentration in the TS or the TDLN. For simplicity, we assume linear pharmacokinetics so that, for some scaling factor f_A, we have that

$$\frac{dA}{dt} = \underbrace{\sum_{j=1}^{n} \xi_j^A f_A \frac{\theta(t-t_j) - \theta(t-t_j-\Delta_A)}{\Delta_A}}_{\text{infusion}} - \underbrace{d_{AC} AC}_{\text{depletion due to killing } C} - \underbrace{d_A A}_{\text{degradation}}, \tag{2.33}$$

$$\begin{aligned}\frac{dA^{\text{LN}}}{dt} = &\underbrace{\sum_{j=1}^{n} \xi_j^A \frac{\theta(t-t_j) - \theta(t-t_j-\Delta_A)}{\Delta_A}}_{\text{infusion}} - \underbrace{d_{A^{\text{LN}}L_8} A^{\text{LN}} L_8}_{\text{depletion due to killing } L_8} - \underbrace{d_{A^{\text{LN}}L_1} A^{\text{LN}} L_1}_{\text{depletion due to killing } L_1} \\ &- \underbrace{d_{A^{\text{LN}}L_2} A^{\text{LN}} L_2}_{\text{depletion due to killing } L_2} - \underbrace{d_{A^{\text{LN}}L_r} A^{\text{LN}} L_r}_{\text{depletion due to killing } L_r} - \underbrace{d_A A^{\text{LN}}}_{\text{degradation}}.\end{aligned} \tag{2.34}$$

2.2.30 Model Reduction via QSSA

The model parameters are listed in Table 2 and are estimated in Appendix A. We note that the degradation rates of cytokines and DAMPs are generally several orders of magnitude higher than those of immune and cancer cells. Specifically, IL-2, IL-4, IFN-γ, TNF, and TGF-β evolve on much faster timescales due to their comparatively rapid degradation, causing them to reach equilibrium significantly quicker than other species in the model. Consequently, we apply a quasi-steady state approximation (QSSA) by setting (2.24), (2.25), (2.28), (2.2.26), and (2.2.27) to zero and solving for I_2, I_4, I_γ, I_α, and I_β as functions of the remaining model variables and parameters. This simplification introduces minimal impact on the system's dynamics beyond a brief transient phase [106], and we support its validity by noting that system trajectories exhibit negligible variation under nearby parameter sets [36]. Implementing the QSSA results in

$$\frac{dI_2}{dt} = 0 \implies I_2 = \frac{1}{d_{I_2}} \left[\left(\lambda_{I_2T_8} T_8 + \lambda_{I_2T_1} T_1\right) \frac{1}{1 + T_r/K_{I_2T_r}} \right], \tag{2.35}$$

$$\frac{dI_4}{dt} = 0 \implies I_4 = \frac{1}{d_{I_4}} \left[\lambda_{I_4T_2} T_2 \right], \tag{2.36}$$

$$\frac{dI_\gamma}{dt} = 0 \implies I_\gamma = \frac{1}{d_{I_\gamma}} \left[\left(\lambda_{I_\gamma T_1} T_1 + \lambda_{I_\gamma K} K\right) \frac{1}{1 + T_r/K_{I_\gamma T_r}} + \lambda_{I_\gamma T_8} T_8 \right], \tag{2.37}$$

$$\frac{dI_\alpha}{dt} = 0 \implies I_\alpha = \frac{1}{d_{I_\alpha}} \left(\lambda_{I_\alpha T_8} T_8 + \lambda_{I_\alpha T_1} T_1 + \lambda_{I_\alpha K} K + \lambda_{I_\alpha M_1} M_1 + \lambda_{I_\alpha D} D\right), \tag{2.38}$$

$$\frac{dI_\beta}{dt} = 0 \implies I_\beta = \frac{1}{d_{I_\beta}} \left(\lambda_{I_\beta T_r} T_r + \lambda_{I_\beta C} C + \lambda_{I_\beta M_2} M_2 + \lambda_{I_\beta K} K\right). \tag{2.39}$$

We note that this reduction holds since IFN-γ (the slowest fast species) still evolves much faster than any slow species in the model [106].

2.3 Model Parameters

The model parameters are in Table 2 as estimated in Appendix A.

Parameter	Description	Value	Unit	Reference
ζ_{DH}	Rate of maturation of D by H	8.831	day^{-1}	est.
ζ_{DR}	Rate of maturation of D by R	0.883	day^{-1}	est.
$\zeta_{L_8D_L}$	Rate of activation of $T_0^8 \to L_8$ by D_L	1.103×10^{-14}	$(\text{cell cm}^{-3})^{-1}\text{day}^{-1}$	est.
$\zeta_{T_8L_8}$	Migration of L_8 to the TS	2.891×10^{-2}	day^{-1}	est.
$\zeta_{L_1D_L}$	Rate of activation of $T_0^4 \to L_1$ by D_L	2.967×10^{-14}	$(\text{cell cm}^{-3})^{-1}\text{day}^{-1}$	est.
$\zeta_{L_2D_L}$	Rate of activation of $T_0^4 \to L_2$ by D_L	1.517×10^{-14}	$(\text{cell cm}^{-3})^{-1}\text{day}^{-1}$	est.
$\zeta_{T_1L_1}$	Migration of L_1 to the TS	2.816×10^{-2}	day^{-1}	est.
$\zeta_{T_2L_2}$	Migration of L_2 to the TS	2.898×10^{-2}	day^{-1}	est.
$\zeta_{L_rD_L}$	Rate of activation of $L_0^r \to L_r$ by D_L	1.970×10^{-11}	$(\text{cell cm}^{-3})^{-1}\text{day}^{-1}$	est.
$\zeta_{T_rL_r}$	Migration of L_r to the TS	1.098×10^{-2}	day^{-1}	est.
$\zeta_{M_1I_\gamma}$	Rate of polarisation of $M_0 \to M_1$ by I_γ	5.371×10^{-1}	day^{-1}	[107] est.
$\zeta_{M_1I_\alpha}$	Rate of polarisation of $M_0 \to M_1$ by I_α	4.613×10^{-1}	day^{-1}	[107] est.
$\zeta_{M_2I_4}$	Rate of polarisation of $M_0 \to M_2$ by I_4	3.165×10^{-1}	day^{-1}	[107] est.
$\zeta_{M_2I_{10}}$	Rate of polarisation of $M_0 \to M_2$ by I_{10}	2.197×10^{-1}	day^{-1}	[107] est.
ζ_{MI_α}	Rate of polarisation of $M_2 \to M_1$ by I_α	2.154×10^{-2}	day^{-1}	[107] est.
ζ_{MI_β}	Rate of polarisation of $M_1 \to M_2$ by I_β	1.337×10^{-2}	day^{-1}	[107] est.
ζ_{MI_γ}	Rate of polarisation of $M_2 \to M_1$ by I_γ	2.585×10^{-2}	day^{-1}	[107] est.
ζ_{KI_2}	Rate of activation of K by I_2	2.385×10^{-1}	day^{-1}	[107] est.
$\zeta_{KI_{12}}$	Rate of activation of K by I_{12}	2.297×10^{-1}	day^{-1}	[107] est.
V_{TS}	Volume of the TS	51	cm^3	[108]
V_{LN}	Volume of the TDLN	1.85×10^{-1}	cm^3	[109]
τ_m	Time for D to travel to the TDLN	0.75	day	[36, 110] est.
τ_8	Time for L_8 to complete clonal expansion	4.85	day	est.
N_8	Number of cell divisions of L_8 to complete clonal expansion	10	dimensionless	[36, 111, 112]
τ_a	Time for L_8 to travel to the TS	0.27	day	[113]
τ_1	Time for L_1 to complete clonal expansion	4.13	day	[36]
N_1	Number of cell divisions of L_1 to complete clonal expansion	9	dimensionless	[114] est.
τ_b	Time for L_1 to travel to the TS	0.27	day	[113]
τ_2	Time for L_2 to complete clonal expansion	4.13	day	[36]
N_2	Number of cell divisions of L_2 to complete clonal expansion	9	dimensionless	[114] est.
τ_c	Time for L_2 to travel to the TS	0.27	day	[113]
τ_r	Time for L_r to complete clonal expansion	2.87	day	[36]

N_r	Number of cell divisions of L_r to complete clonal expansion	6	dimensionless	[115] est.
τ_d	Time for L_r to travel to the TS	0.27	day	[113]
r_C	Growth constant of C	0.534	day^{-1}	est.
λ_{CP}	Rate of apoptosis of C by P	2.857×10^{-1}	day^{-1}	est.
λ_{CA}	Rate of apoptosis of C by A	7.00×10^{-1}	day^{-1}	est.
ν_{CP}	Rate of necrosis of C by P	1.429×10^{-2}	day^{-1}	est.
λ_{CT_8}	Rate of lysis of C by T_8	4.00×10^{-8}	$(\text{cell/cm}^3)^{-1}\text{day}^{-1}$	est.
λ_{CT_1}	Rate of lysis of C by T_1	1.25×10^{-9}	$(\text{cell/cm}^3)^{-1}\text{day}^{-1}$	est.
λ_{CK}	Rate of lysis of C by K	4.00×10^{-8}	$(\text{cell/cm}^3)^{-1}\text{day}^{-1}$	est.
λ_{CI_α}	Rate of lysis of C by I_α	0.704	day^{-1}	est.
λ_{CI_γ}	Rate of lysis of C by I_γ	14.08×10^{-2}	day^{-1}	est.
λ_{NH}	Rate of H release by N	1.263×10^{-12}	$(\text{g/cell})\,\text{day}^{-1}$	est.
λ_{NR}	Rate of R release by N	2.128×10^{-13}	$(\text{g/cell})\,\text{day}^{-1}$	est.
$\lambda_{D_L D}$	Rate of D migration to TDLN	6.114×10^{-1}	day^{-1}	est.
$\lambda_{T_8 I_2}$	Rate of proliferation of T_8 by I_2	9×10^{-4}	day^{-1}	est.
$\lambda_{T_1 I_2}$	Rate of proliferation of T_1 by I_2	7.970×10^{-4}	day^{-1}	est.
$\lambda_{T_2 I_4}$	Rate of proliferation of T_2 by I_4	3.985×10^{-4}	day^{-1}	est.
$\lambda_{T_r I_\beta}$	Rate of proliferation of T_r by I_β	6.30×10^{-3}	day^{-1}	est.
$\lambda_{K I_2}$	Rate of proliferation of K by I_2	1.518×10^{-3}	day^{-1}	est.
$\lambda_{K I_{12}}$	Rate of proliferation of K by I_{12}	1.462×10^{-3}	day^{-1}	est.
$\lambda_{I_2 T_1}$	Rate of production of I_2 by T_1	9.957×10^{-14}	$(\text{g/cell})\,\text{day}^{-1}$	[107] est.
$\lambda_{I_2 T_8}$	Rate of production of I_2 by T_8	3.399×10^{-14}	$(\text{g/cell})\,\text{day}^{-1}$	[107] est.
$\lambda_{I_4 T_2}$	Rate of production of I_4 by T_2	8.749×10^{-15}	$(\text{g/cell})\,\text{day}^{-1}$	est.
$\lambda_{I_{10} T_r}$	Rate of production of I_{10} by T_r	2.204×10^{-15}	$(\text{g/cell})\,\text{day}^{-1}$	[107] est.
$\lambda_{I_{10} M_2}$	Rate of production of I_{10} by M_2	4.667×10^{-15}	$(\text{g/cell})\,\text{day}^{-1}$	[107] est.
$\lambda_{I_{10} C}$	Rate of production of I_{10} by C	2.334×10^{-15}	$(\text{g/cell})\,\text{day}^{-1}$	[107] est.
$\lambda_{I_{12} D}$	Rate of production of I_{12} by D	7.05×10^{-18}	$(\text{g/cell})\,\text{day}^{-1}$	[107] est.
$\lambda_{I_{12} M_1}$	Rate of production of I_{12} by M_1	8.03×10^{-18}	$(\text{g/cell})\,\text{day}^{-1}$	[107] est.
$\lambda_{I_\gamma T_1}$	Rate of production of I_γ by T_1	4.202×10^{-17}	$(\text{g/cell})\,\text{day}^{-1}$	[107] est.
$\lambda_{I_\gamma K}$	Rate of production of I_γ by K	2.224×10^{-15}	$(\text{g/cell})\,\text{day}^{-1}$	[107] est.
$\lambda_{I_\gamma T_8}$	Rate of production of I_γ by T_8	6.001×10^{-17}	$(\text{g/cell})\,\text{day}^{-1}$	[107] est.
$\lambda_{I_\alpha T_8}$	Rate of production of I_α by T_8	2.712×10^{-17}	$(\text{g/cell})\,\text{day}^{-1}$	[107] est.
$\lambda_{I_\alpha T_1}$	Rate of production of I_α by T_1	4.483×10^{-17}	$(\text{g/cell})\,\text{day}^{-1}$	[107] est.
$\lambda_{I_\alpha K}$	Rate of production of I_α by K	4.729×10^{-17}	$(\text{g/cell})\,\text{day}^{-1}$	[107] est.
$\lambda_{I_\alpha M_1}$	Rate of production of I_α by M_1	1.643×10^{-17}	$(\text{g/cell})\,\text{day}^{-1}$	[107] est.
$\lambda_{I_\alpha D}$	Rate of production of I_α by D	8.256×10^{-17}	$(\text{g/cell})\,\text{day}^{-1}$	[107] est.
$\lambda_{I_\beta T_r}$	Rate of production of I_β by T_r	1.191×10^{-12}	$(\text{g/cell})\,\text{day}^{-1}$	[107] est.
$\lambda_{I_\beta C}$	Rate of production of I_β by C	2.057×10^{-13}	$(\text{g/cell})\,\text{day}^{-1}$	est.
$\lambda_{I_\beta M_2}$	Rate of production of I_β by M_2	1.48×10^{-12}	$(\text{g/cell})\,\text{day}^{-1}$	[107] est.
$\lambda_{I_\beta K}$	Rate of production of I_β by K	1.007×10^{-12}	$(\text{g/cell})\,\text{day}^{-1}$	[107] est.
f_P	P/P^{LN} dose scaling factor	1.043×10^{-8}	$\text{g cm}^{-3}\ \text{mg}^{-1}$	[116] est.
f_A	A/A^{LN} dose scaling factor	4.229×10^{-8}	$\text{g cm}^{-3}\ \text{mg}^{-1}$	[116] est.
K_{CP}	Half-saturation of P for C	3.064×10^{-7}	g cm^{-3}	[116] est.
K_{CA}	Half-saturation of A for C	3.713×10^{-6}	g cm^{-3}	[116] est.
K_{CI_α}	Half-saturation of I_α for C	2.62×10^{-12}	g cm^{-3}	[117] est.
K_{CI_γ}	Half-saturation of I_γ for C	5.2×10^{-11}	g cm^{-3}	[117] est.

K_{DH}	Half-saturation of H for D	6.69×10^{-8}	g cm^{-3}	[118] est.
K_{DR}	Half-saturation of H for R	4.5×10^{-8}	g cm^{-3}	[119] est.
$K_{T_8I_2}$	Half-saturation of I_2 for T_8	2.91×10^{-11}	g cm^{-3}	[120] est.
$K_{T_1I_2}$	Half-saturation of I_2 for T_1	2.91×10^{-11}	cell cm^{-3}	[121] est.
$K_{T_2I_4}$	Half-saturation of I_4 for T_2	9.46×10^{-12}	g cm^{-3}	[122] est.
$K_{T_rI_\beta}$	Half-saturation of I_β for T_r	1.75×10^{-8}	g cm^{-3}	[123, 124] est.
$K_{M_1I_\gamma}$	Half-saturation of I_γ for M_1	5.2×10^{-11}	g cm^{-3}	[117] est.
$K_{M_1I_\alpha}$	Half-saturation of I_α for M_1	2.62×10^{-12}	g cm^{-3}	[117] est.
$K_{M_2I_4}$	Half-saturation of I_4 for M_2	9.46×10^{-12}	g cm^{-3}	[122] est.
$K_{M_2I_{10}}$	Half-saturation of I_{10} for M_2	1.1×10^{-8}	g cm^{-3}	[125, 126] est.
$K_{M_2I_\beta}$	Half-saturation of I_β for M_2	1.75×10^{-8}	g cm^{-3}	[123, 124] est.
K_{KI_2}	Half-saturation of I_2 for K	2.91×10^{-11}	g cm^{-3}	[120] est.
$K_{KI_{12}}$	Half-saturation of I_{12} for K	3.1×10^{-12}	g cm^{-3}	[127] est.
C_0	Carrying capacity of C	1.75×10^{8}	cell cm^{-3}	est.
$K_{T_8I_\beta}$	Inhibition constant of T_8 elimination of C by I_β	1.75×10^{-8}	g cm^{-3}	[123, 124] est.
$K_{T_8T_r}$	Inhibition constant of T_8 elimination of C by T_r	1.25×10^{5}	cell cm^{-3}	[121] est.
$K_{T_1T_r}$	Inhibition constant of T_1 elimination of C by T_r	1.25×10^{5}	cell cm^{-3}	[121] est.
K_{KI_β}	Inhibition constant for K elimination of C by I_β	1.75×10^{-8}	g cm^{-3}	[123, 124] est.
K_{KT_r}	Inhibition constant for K elimination of C by T_r	1.25×10^{5}	cell cm^{-3}	[121] est.
$K_{DI_{10}}$	Inhibition constant for D_0 maturation by I_{10}	1.1×10^{-8}	g cm^{-3}	[125, 126] est.
K_{DI_β}	Inhibition constant for D_0 maturation by I_β	1.75×10^{-8}	g cm^{-3}	[123, 124] est.
$K_{T_0^8L_r}$	Inhibition constant for T_0^8 activation by L_r	1.91×10^{8}	cell cm^{-3}	[121] est.
$K_{L_8P^{\mathrm{LN}}}$	Inhibition constant of activated CD8+ T cell proliferation by P^{LN}	4.995×10^{-7}	(g cm^{-3}) day	[116] est.
$K_{L_8A^{\mathrm{LN}}}$	Inhibition constant of activated CD8+ T cell proliferation by A^{LN}	6.053×10^{-6}	(g cm^{-3}) day	[116] est.
$K_{L_8L_r}$	Inhibition constant for activated CD8+ T cell proliferation by L_r	1.91×10^{8}	cell cm^{-3}	[121] est.
$K_{T_8I_{10}}$	Inhibition constant of T_8 death by I_{10}	1.1×10^{-8}	g cm^{-3}	[125, 126] est.
$K_{T_0^4L_r}$	Inhibition constant for T_0^4 activation by L_r	1.91×10^{8}	cell cm^{-3}	[121] est.
$K_{L_1P^{\mathrm{LN}}}$	Inhibition constant of activated Th1 cell proliferation by P^{LN}	1.266×10^{-6}	(g cm^{-3}) day	[116] est.
$K_{L_1A^{\mathrm{LN}}}$	Inhibition constant of activated Th1 cell proliferation by A^{LN}	1.534×10^{-5}	(g cm^{-3}) day	[116] est.
$K_{L_1L_r}$	Inhibition constant for activated Th1 cell proliferation by L_r	1.91×10^{8}	cell cm^{-3}	[121] est.
$K_{L_2P^{\mathrm{LN}}}$	Inhibition constant of activated Th2 cell proliferation by P^{LN}	1.266×10^{-6}	(g cm^{-3}) day	[116] est.

$K_{L_2A^{\mathrm{LN}}}$	Inhibition constant of activated Th2 cell proliferation by A^{LN}	1.534×10^{-5}	(g cm^{-3}) day	[116] est.
$K_{L_rP^{\mathrm{LN}}}$	Inhibition constant of activated Treg proliferation by P^{LN}	8.795×10^{-7}	(g cm^{-3}) day	[116] est.
$K_{L_rA^{\mathrm{LN}}}$	Inhibition constant of activated Treg proliferation by A^{LN}	1.066×10^{-5}	(g cm^{-3}) day	[116] est.
$K_{I_2T_r}$	Inhibition constant of production of I_2 by T_r	1.25×10^{5}	cell cm^{-3}	[121] est.
$K_{I_\gamma T_r}$	Inhibition constant of production of I_γ by T_r	1.25×10^{5}	cell cm^{-3}	[121] est.
$\mathcal{A}_{D_0}$	Source of D_0	7.20×10^{5}	cell cm^{-3} day^{-1}	[128] est.
$\mathcal{A}_{T}$	Source of T_r	3.572×10^{5}	cell cm^{-3} day^{-1}	est.
$\mathcal{A}_{T_8^0}$	Source of T_8^0	2.486×10^{6}	cell cm^{-3} day^{-1}	est.
$\mathcal{A}_{T_4^0}$	Source of T_4^0	2.547×10^{6}	cell cm^{-3} day^{-1}	est.
$\mathcal{A}_{M_0}$	Source of M_0	5.551×10^{5}	cell cm^{-3} day^{-1}	est.
$\mathcal{A}_{K_0}$	Source of K_0	1.362×10^{5}	cell cm^{-3} day^{-1}	est.
d_N	Degradation rate of N	4.81×10^{1}	day^{-1}	est.
d_H	Degradation rate of H	5.55	day^{-1}	[129]
d_R	Degradation rate of R	1.39	day^{-1}	[130]
d_{D_0}	Degradation rate of D_0	3.57×10^{-2}	day^{-1}	[131]
d_D	Degradation rate of D	3.15×10^{-1}	day^{-1}	[132, 133]
d_{D_L}	Degradation rate of D_L	3.15×10^{-1}	day^{-1}	[132]
$d_{T_8^0}$	Degradation rate of T_8^0	3.22×10^{-2}	day^{-1}	[134]
d_{L_8}	Degradation rate of L_8	9.0×10^{-3}	day^{-1}	[135]
d_{T_8}	Degradation rate of T_8	9.0×10^{-3}	day^{-1}	[135]
$d_{T_4^0}$	Degradation rate of T_4^0	4.03×10^{-2}	day^{-1}	[134]
d_{L_1}	Degradation rate of L_1	7.97×10^{-3}	day^{-1}	[135]
d_{T_1}	Degradation rate of T_1	7.97×10^{-3}	day^{-1}	[135]
d_{L_2}	Degradation rate of L_2	7.97×10^{-3}	day^{-1}	[135]
d_{T_2}	Degradation rate of T_2	7.97×10^{-3}	day^{-1}	[135]
$d_{L_0^r}$	Degradation rate of L_0^r	2.2×10^{-3}	day^{-1}	[136]
d_{L_r}	Degradation rate of L_r	6.3×10^{-2}	day^{-1}	[137]
d_{T_r}	Degradation rate of T_r	6.3×10^{-2}	day^{-1}	[137]
d_{M_0}	Degradation rate of M_0	7.3×10^{-1}	day^{-1}	[138]
d_{M_1}	Degradation rate of M_1	9.9×10^{-1}	day^{-1}	[138, 139]
d_{M_2}	Degradation rate of M_2	1.35×10^{-1}	day^{-1}	[138]
d_{K_0}	Degradation rate of K_0	6.93×10^{-2}	day^{-1}	[112, 140]
d_K	Degradation rate of K	6.93×10^{-2}	day^{-1}	[112, 140]
d_{I_2}	Degradation rate of I_2	1.446×10^{2}	day^{-1}	[141, 142]
d_{I_4}	Degradation rate of I_4	5.253×10^{1}	day^{-1}	[143]
$d_{I_{10}}$	Degradation rate of I_{10}	6.16	day^{-1}	[144, 145]
$d_{I_{12}}$	Degradation rate of I_{12}	2.23	day^{-1}	[146]
d_{I_γ}	Degradation rate of I_γ	3.327×10^{1}	day^{-1}	[147]
d_{I_α}	Degradation rate of I_α	5.484×10^{1}	day^{-1}	[148, 149]
d_{I_β}	Degradation rate of I_β	4.991×10^{2}	day^{-1}	[150, 151]
d_{PC}	Depletion rate of P by killing C	5.196×10^{-7}	(cell/cm^3)$^{-1}$day^{-1}	est.
d_P	Degradation rate of P and P^{LN}	1.68	day^{-1}	[152]

$d_{P^{\mathrm{LN}}L_8}$	Depletion rate of P^{LN} by killing L_8	3.347×10^{-9}	$(\mathrm{cell/cm^3})^{-1}\mathrm{day}^{-1}$	est.
$d_{P^{\mathrm{LN}}L_1}$	Depletion rate of P^{LN} by killing L_1	3.012×10^{-9}	$(\mathrm{cell/cm^3})^{-1}\mathrm{day}^{-1}$	est.
$d_{P^{\mathrm{LN}}L_2}$	Depletion rate of P^{LN} by killing L_2	3.012×10^{-9}	$(\mathrm{cell/cm^3})^{-1}\mathrm{day}^{-1}$	est.
$d_{P^{\mathrm{LN}}L_r}$	Depletion rate of P^{LN} by killing L_r	2.008×10^{-9}	$(\mathrm{cell/cm^3})^{-1}\mathrm{day}^{-1}$	est.
d_{AC}	Depletion rate of A by killing C	5.184×10^{-8}	$(\mathrm{cell/cm^3})^{-1}\mathrm{day}^{-1}$	est.
d_A	Degradation rate of A and A^{LN}	1.676×10^{-1}	day^{-1}	[153] est.
$d_{A^{\mathrm{LN}}L_8}$	Depletion rate of A^{LN} by killing L_8	3.339×10^{-10}	$(\mathrm{cell/cm^3})^{-1}\mathrm{day}^{-1}$	est.
$d_{A^{\mathrm{LN}}L_1}$	Depletion rate of A^{LN} by killing L_1	3.005×10^{-10}	$(\mathrm{cell/cm^3})^{-1}\mathrm{day}^{-1}$	est.
$d_{A^{\mathrm{LN}}L_2}$	Depletion rate of A^{LN} by killing L_2	3.005×10^{-10}	$(\mathrm{cell/cm^3})^{-1}\mathrm{day}^{-1}$	est.
$d_{A^{\mathrm{LN}}L_r}$	Depletion rate of A^{LN} by killing L_r	2.003×10^{-10}	$(\mathrm{cell/cm^3})^{-1}\mathrm{day}^{-1}$	est.

Table 2: Parameter values for the model. est. denotes estimated parameters.

3 Initial Conditions and Steady States

Biologically, we assumed a steady state occurred in Stage IV HGSOC patients due to a maladaptive TME where immune regulation becomes dysfunctional. We chose Stage III HGSOC patients as our initial condition, as most patients are diagnosed at this stage with the cell steady states and initial conditions to be as in Table 3. The justification for the choice of these values is shown in Appendix A.1.

Table 3: Cell steady states and initial conditions for the model. All values are in units of cells/cm^3.

Cell	Initial Condition	Steady State	Cell	Initial Condition	Steady State
C	9.60×10^6	2.91×10^7	N	9.70×10^4	2.94×10^5
D_0	6.60×10^5	5.76×10^5	D	6.46×10^5	7.55×10^5
D_L	2.73×10^8	3.19×10^8	T_0^8	4.35×10^7	7.72×10^7
T_8	8.61×10^4	8.59×10^4	L_8	3.40×10^7	3.51×10^6
T_0^4	4.22×10^7	6.32×10^7	L_1	2.59×10^7	4.10×10^6
T_1	5.64×10^4	5.52×10^4	L_2	2.04×10^6	4.10×10^6
T_2	7.18×10^4	5.68×10^4	L_0^r	3.54×10^7	4.21×10^7
L_r	1.61×10^8	1.91×10^8	T_r	1.30×10^5	1.25×10^5
M_0	3.50×10^5	3.62×10^5	M_1	1.97×10^5	1.98×10^5
M_2	6.19×10^5	7.02×10^5	K_0	1.47×10^5	4.49×10^5
K	1.86×10^6	1.55×10^6			

We chose the DAMP steady states and initial conditions to be as in Table 4. The justification for these values is explained in Appendix A.2.

Table 4: DAMP steady states and initial conditions for the model. All values are in units of g/cm^3.

DAMP	Initial Condition	Steady State
H	3.15×10^{-8}	6.69×10^{-8}
R	2.00×10^{-8}	4.50×10^{-8}

We choose the cytokine steady states and initial conditions as in Table 5. The choice of these values is explained in Appendix A.3.

Table 5: Cytokine initial conditions and steady states for the model. All values are in units of g/cm^3.

Cytokine	Initial Condition	Steady State
I_2	3.05×10^{-11}	2.91×10^{-11}
I_4	8.11×10^{-12}	9.46×10^{-12}
I_{10}	1.03×10^{-8}	1.16×10^{-8}
I_{12}	1.96×10^{-11}	3.10×10^{-12}
I_α	2.72×10^{-12}	2.62×10^{-12}
I_γ	6.11×10^{-11}	5.20×10^{-11}
I_β	1.48×10^{-8}	1.75×10^{-8}

4 Results

We now aim to optimise neoadjuvant paclitaxel and carboplatin therapy in advanced HGSOC. For simplicity, we assume that paclitaxel and carboplatin are given at a constant dosage and that the spacing between consecutive infusions is constant. We also assume that the patient has paclitaxel and carboplatin at $t = 0$ days, and we consider a treatment regimen lasting for 12 weeks so that the time for the latest allowed infusion occurs before $t = 84$ days, and simulate to 84 days. In our optimisation, we consider the following four objectives: efficacy, tumour volume reduction (TVR), efficiency, and toxicity.

First, we use the Calvert formula to determine the appropriate dose of carboplatin (in mg) based on the desired AUC (in mg/mL min) and the patient's glomerular filtration rate (GFR) (in mL/min/1.73m^2), taking into account the patient's renal function [154]:

$$\text{Carboplatin Dose (mg)} = (\text{GFR} + 25) \times \text{AUC}.$$

The mean GFR in OC patients was found to be 73.2 mL/min/1.73m^2 [155], hence we take

$$\text{Carboplatin Dose (mg)} = 98.2 \times \text{AUC}.$$

We define $V(t) = C(t) + N(t)$ as the total cancer concentration at time t without treatment, and define $V(\xi_P; \eta_P; \xi_A; \eta_A, t) = C(\xi_P; \eta_P; \xi_A; \eta_A, t) + N(\xi_P; \eta_P; \xi_A; \eta_A, t)$ as the total cancer concentration at time t with treatment with paclitaxel doses of ξ_P mg/m^2 at a dosing interval of η_P days and carboplatin doses with a target AUC of ξ_A mg/mL min at a dosing interval of η_A days. We define the efficacy at time t from this regimen to be

$$\text{efficacy}(\xi_P; \eta_P; \xi_A; \eta_A, t) := \left(1 - \frac{\int_0^t V(\xi_P; \eta_P; \xi_A; \eta_A, s)\ ds}{\int_0^t V(s)\ ds}\right) \times 100\%. \tag{4.1}$$

We also define the TVR similarly, as

$$\text{TVR}(\xi_P; \eta_P; \xi_A; \eta_A, t) := \left(1 - \frac{\int_0^t V(\xi_P; \eta_P; \xi_A; \eta_A, s)\ ds}{V(0)t}\right) \times 100\%. \tag{4.2}$$

In particular, the efficacy represents the extent of tumour density shrinkage throughout its growth course in comparison to no treatment, whereas the TVR reveals how much the tumour density has

reduced since the commencement of treatment. We see that the TVR and efficacy are linearly related via the formula

$$\text{efficacy}(\xi_P;\eta_P;\xi_A;\eta_A,t) = \left(1 - \frac{V(0)t}{\int_0^t V(s)\ ds}\right) \times 100\% + \frac{V(0)t}{\int_0^t V(s)\ ds} \times \text{TVR}\left(\xi_P;\eta_P;\xi_A;\eta_A,t\right), \quad (4.3)$$

so that an increase in treatment efficacy results in increased TVR, and vice versa. As such, we calculate only the TVR, and the corresponding treatment efficacy can be calculated via (4.3).

We can also consider the efficiency of the treatment regimen, given by

$$\begin{aligned}\text{efficiency}(\xi_P;\eta_P;\xi_A;\eta_A,t) := &\frac{\text{TVR}(\xi_P;\eta_P;\xi_A;\eta_A,t)}{1.73 \times \xi_P \times (1 + \lfloor t/\eta_P \rfloor) + 98.2 \times \xi_A \times (1 + \lfloor t/\eta_A \rfloor)} \\ &\div \frac{\text{TVR}(175;21;5;21,t)}{1.73 \times 175 \times (1 + \lfloor t/21 \rfloor) + 98.2 \times 5 \times (1 + \lfloor t/21 \rfloor)},\end{aligned} \quad (4.4)$$

where $1.73 \times \xi_P \times (1 + \lfloor t/\eta_P \rfloor)$ and $98.2 \times \xi_A \times (1 + \lfloor t/\eta_A \rfloor)$ are the total doses of paclitaxel and carboplatin, in mg, administered by time t, respectively, assuming a body surface area of 1.73 m^2 and a GFR of 73.2 mL/min/1.73m^2. The efficiency corresponds to the ratio of the TVR percentage to the total chemotherapy dose administered, comparing the treatment regimen to the standard regimen, with an efficiency greater than 1 denoting a treatment more efficient than the standard regimen and vice versa.

Finally, we can define the toxicity of the treatment regimen, noting that large enough paclitaxel and carboplatin concentrations can potentially cause peripheral neuropathy, bone marrow suppression and cardiotoxicity [156–158]. It was shown in [154] that single-agent carboplatin given at an AUC between 6–8 mg/mL min in previously untreated patients led to manageable haematological toxicity. It was also shown in [159] that a regimen of 550 mg/m^2 of carboplatin and 200 mg/m^2 of paclitaxel, administered triweekly for six courses, represents the maximum tolerated dose for previously untreated OC patients. As such, we assume that the threshold for treatment toxicity is 200 mg/m^2 of paclitaxel and an AUC of 7 mg/mL min of carboplatin every 3 weeks, with higher doses being deemed toxic. To rigorise this notion, we define the toxicity of the treatment regimen as

$$\begin{aligned}\text{toxicity}(\xi_P;\eta_P;\xi_A;\eta_A,t) := \max\Bigg(&\frac{\max_{s\in[0,t]} P(\xi_P;\eta_P;\xi_A;\eta_A,s)}{\max_{s\in[0,t]} P(200;21;7;21,s)}, \frac{\max_{s\in[0,t]} P^{\text{LN}}(\xi_P;\eta_P;\xi_A;\eta_A,s)}{\max_{s\in[0,t]} P^{\text{LN}}(200;21;7;21,s)}, \\ &\frac{\max_{s\in[0,t]} A(\xi_P;\eta_P;\xi_A;\eta_A,s)}{\max_{s\in[0,t]} A(200;21;7;21,s)}, \frac{\max_{s\in[0,t]} A^{\text{LN}}(\xi_P;\eta_P;\xi_A;\eta_A,s)}{\max_{s\in[0,t]} A^{\text{LN}}(200;21;7;21,s)}\Bigg).\end{aligned} \quad (4.5)$$

In particular, $P(\xi_P;\eta_P;\xi_A;\eta_A,s)$ and $A(\xi_P;\eta_P;\xi_A;\eta_A,s)$ denote the concentrations of carboplatin and paclitaxel in the TS at time s, respectively. In particular, the toxicity quantifies the ratio of the maximum paclitaxel and carboplatin concentrations from the regimen to those of the threshold regimen, taking the highest value of this ratio between the TDLN and TS. A toxicity greater than 1 indicates a toxic and unsafe regimen, whereas a toxicity of 1 or less signifies a non-toxic and safe regimen, with lower toxicity values corresponding to safer treatments.

We perform a sweep across the space $\eta_P, \eta_A \in \{7, 14, 21, 28, 42\}$ days. These values are integer factors of 84 days, corresponding to a distinct number of paclitaxel or carboplatin doses administered. This

approach ensures practicality whilst preventing any artefacts that could occur from selecting a treatment regimen that ends at a fixed time of 12 weeks. We consider linearly spaced dosages in the domain $\xi_{\mathrm{P}} \in [0\ \mathrm{mg/m^2}, 200\ \mathrm{mg/m^2}]$ with an increment of 5 $\mathrm{mg/m^2}$ and $\xi_A \in [0\ \mathrm{AUC}, 7\ \mathrm{AUC}]$ with an increment of 0.05 AUC, assuming a patient body surface area of 1.73 $\mathrm{m^2}$ and GFR of 73.2 $\mathrm{mL/min/1.73m^2}$.

Heatmaps of TVR, efficacy, efficiency, and toxicity at 12 weeks for these η_P, η_A, ξ_P and ξ_A values are shown in Appendix B. All simulations were done in MATLAB using the dde23 solver with the initial conditions stated in Section 3 and drug parameters as above.

We can determine the optimal paclitaxel and carboplatin therapies by considering the regimens that achieve an acceptable TVR at 12 weeks, whilst maximising treatment efficiency as much as possible and ensuring toxicity of less than 1. To ensure that the TVR of the optimal treatments is comparable to the SR, we set the threshold TVR to be 75%. Denoting the space of regimens, (P^{reg}, A^{reg}), that satisfy these criteria as $\mathcal{S}^{\mathrm{prac}}$, the optimal regimens, (P^{opt}, A^{opt}), satisfy

$$(P^{\mathrm{opt}}, A^{\mathrm{opt}}) = \underset{\substack{\mathrm{TVR}(P^{\mathrm{reg}};A^{\mathrm{reg}},84)\geq 75\% \\ (P^{\mathrm{reg}};A^{\mathrm{reg}})\in\mathcal{S}^{\mathrm{prac}} \\ \mathrm{toxicity}(P^{\mathrm{reg}};A^{\mathrm{reg}},84)\leq 1}}{\mathrm{argmax}} \ \mathrm{efficiency}\,(P^{\mathrm{reg}}; A^{\mathrm{reg}}, 84)\,. \tag{4.6}$$

Solving leads to the optimal therapies defined in Table 6. We define a cyclic regimen, such as the 21-day cyclic regimen 101, to indicate treatment on day 1, no treatment on day 8 and treatment on day 15, and similarly for 28-day cyclic regimens.

Table 6: Comparison of ξ_P, ξ_A, TVR, efficacy, efficiency and toxicity for the optimal chemotherapy regimens. *Dose given on Day 1 and Day 8. **Dose given on Day 1, 8, 15.

Regimen	ξ_P **(mg/m²)**	ξ_A **(AUC)**	**TVR (%)**	**Efficacy (%)**	**Efficiency**	**Toxicity**
Standard Regimen	175	5.00	75.85	89.86	1.00	0.87
Optimal Triweekly	0	5.75	75.07	89.54	1.39	0.82
Optimal Biweekly	0	3.30	75.46	89.70	1.62	0.50
Optimal Weekly	0	1.40	75.83	89.86	1.92	0.28
Optimal 21-day cycle*	0	2.00	75.16	89.57	2.00	0.37
Optimal 28-day cycle**	0	1.70	75.79	89.84	2.11	0.33

Time traces for total cancer concentration (V) under optimal triweekly, biweekly, weekly, 21-day cycle and 28-day cycle paclitaxel and carboplatin therapies, compared to no treatment, are shown in Figure 3. We can also compare the effect of optimal triweekly, biweekly, weekly, 21-day cyclic and 28-day cyclic regimens against no treatment, on the TME, with time traces of key variables shown in Figure 4. Figure 5 breaks down the treatment regimes into TVR, efficacy, efficiency, and toxicity. For the cycle regimens, we present heatmaps of TVR, efficacy, efficiency, and toxicity in Figure 6.

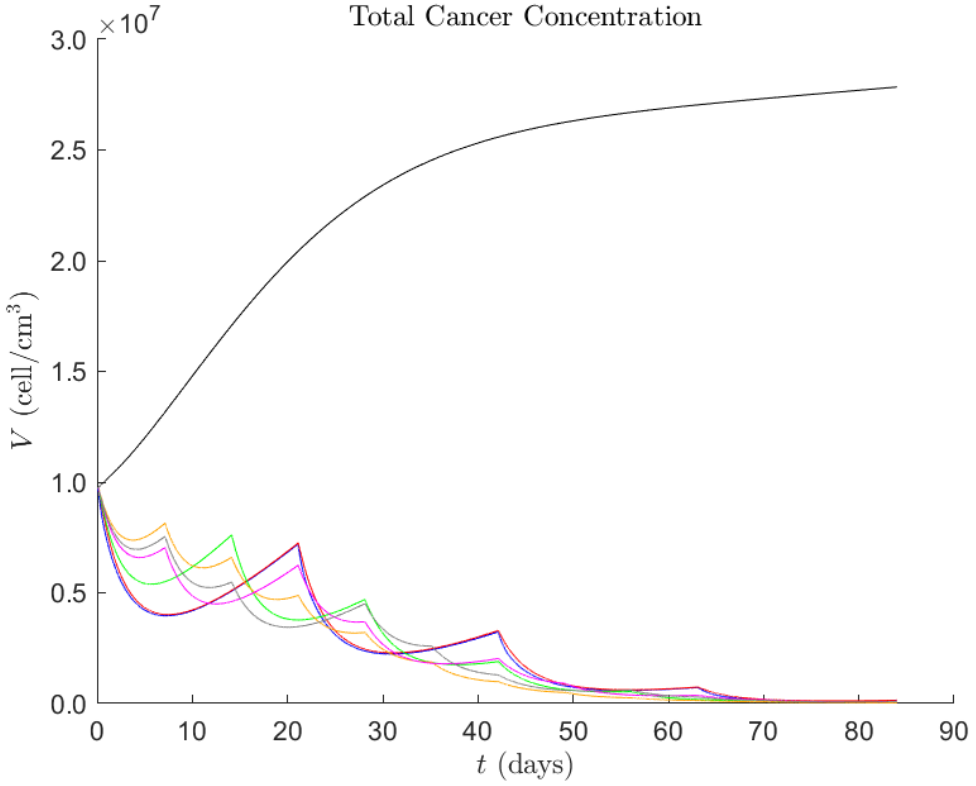

Figure 3: Left: time traces of V up to 84 days from commencement, with no treatment shown in black, SR in blue, optimal triweekly in red, optimal biweekly in green, optimal weekly in orange, optimal 21-day cycle in magenta and optimal 28-day cycle in grey.

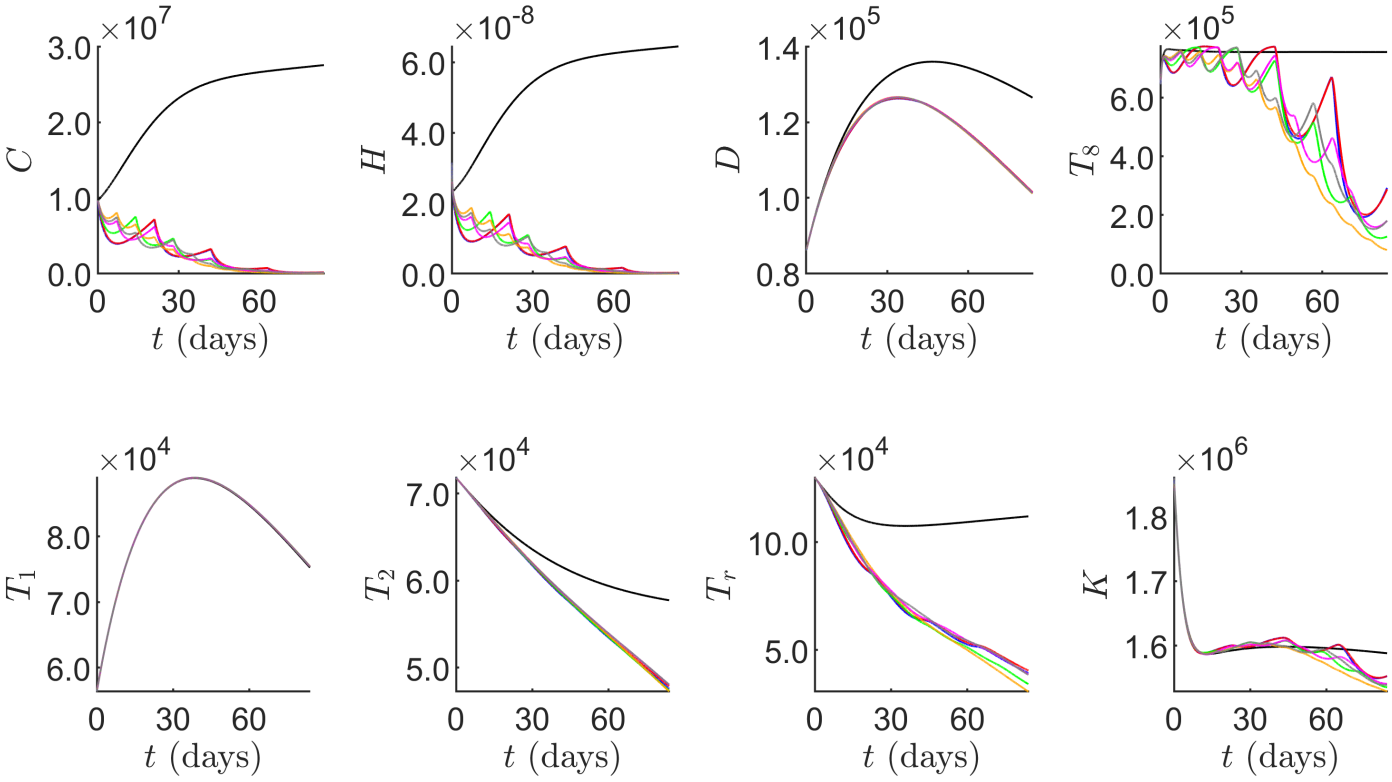

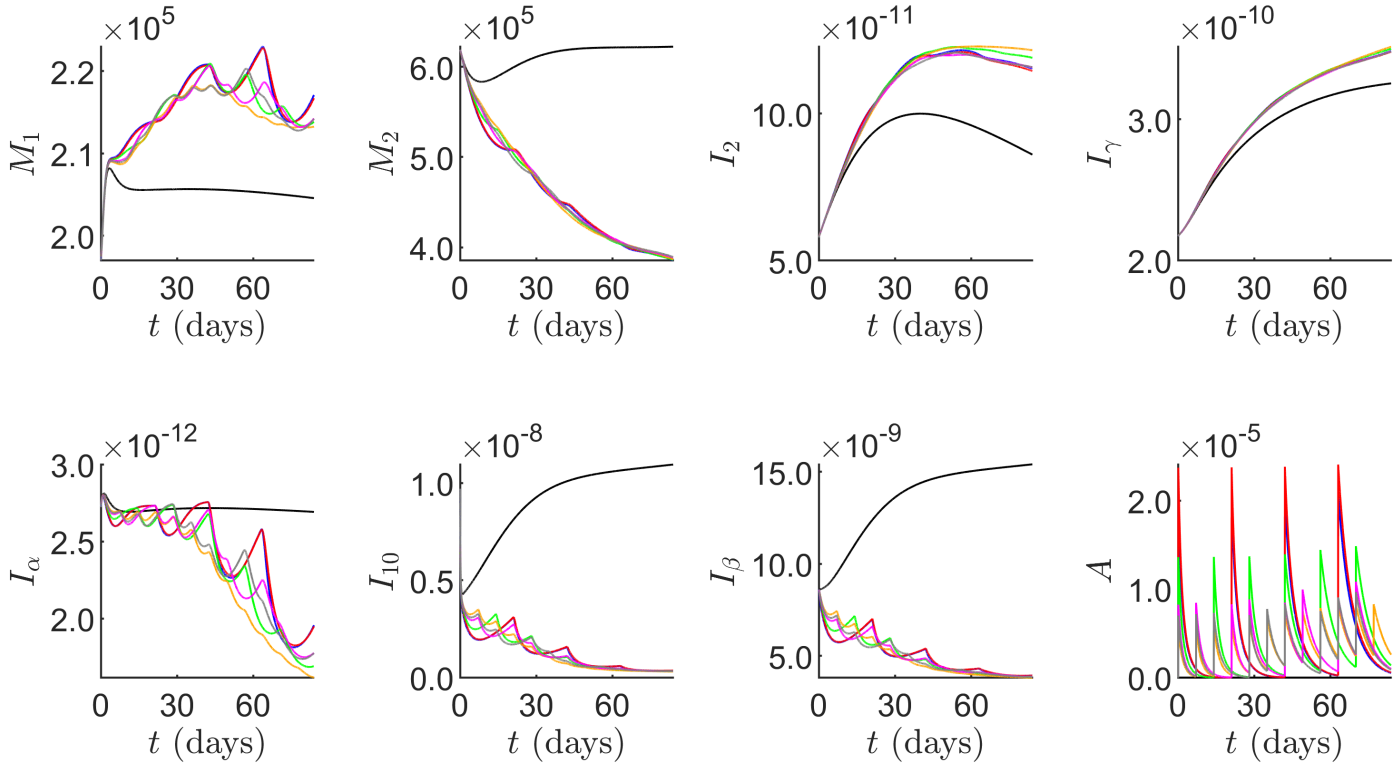

Figure 4: Time traces of notable variables in the model, with the units of the variables as in Table 1. Time traces with no treatment in black, SR in blue, optimal triweekly regimen in red, optimal biweekly regimen in green, optimal weekly regimen in orange, optimal 21-day cycle in magenta and optimal 28-day cycle in grey.

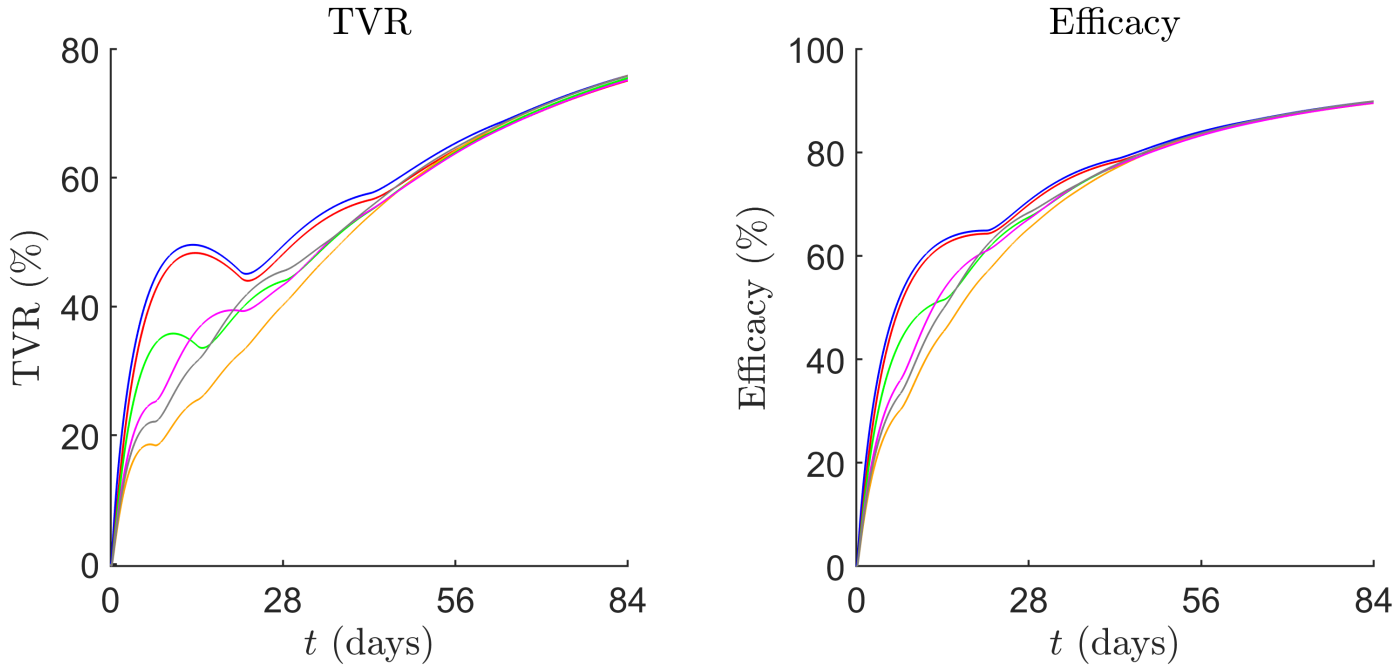

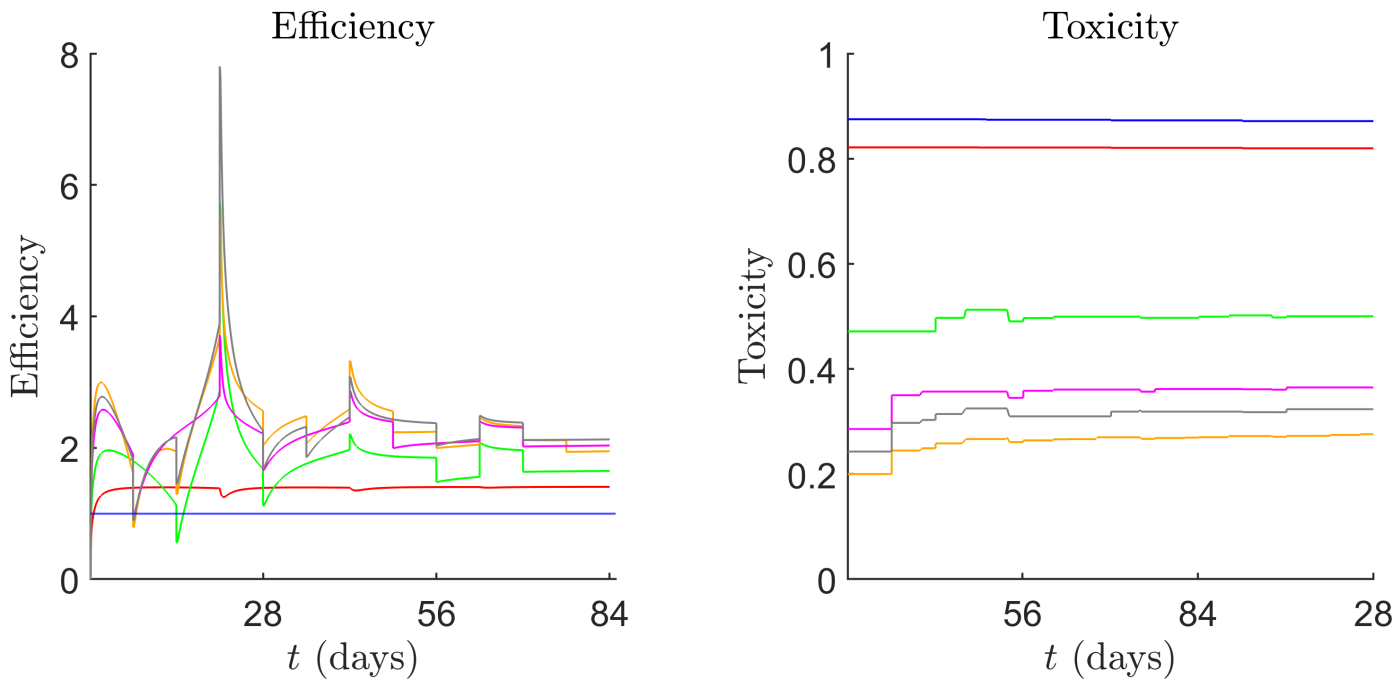

Figure 5: Time traces of TVR, efficacy, efficiency and toxicity. SR in blue, optimal triweekly in red, optimal biweekly in green, optimal weekly in orange, optimal 21-day cycle in magenta and optimal 28-day cycle in grey.

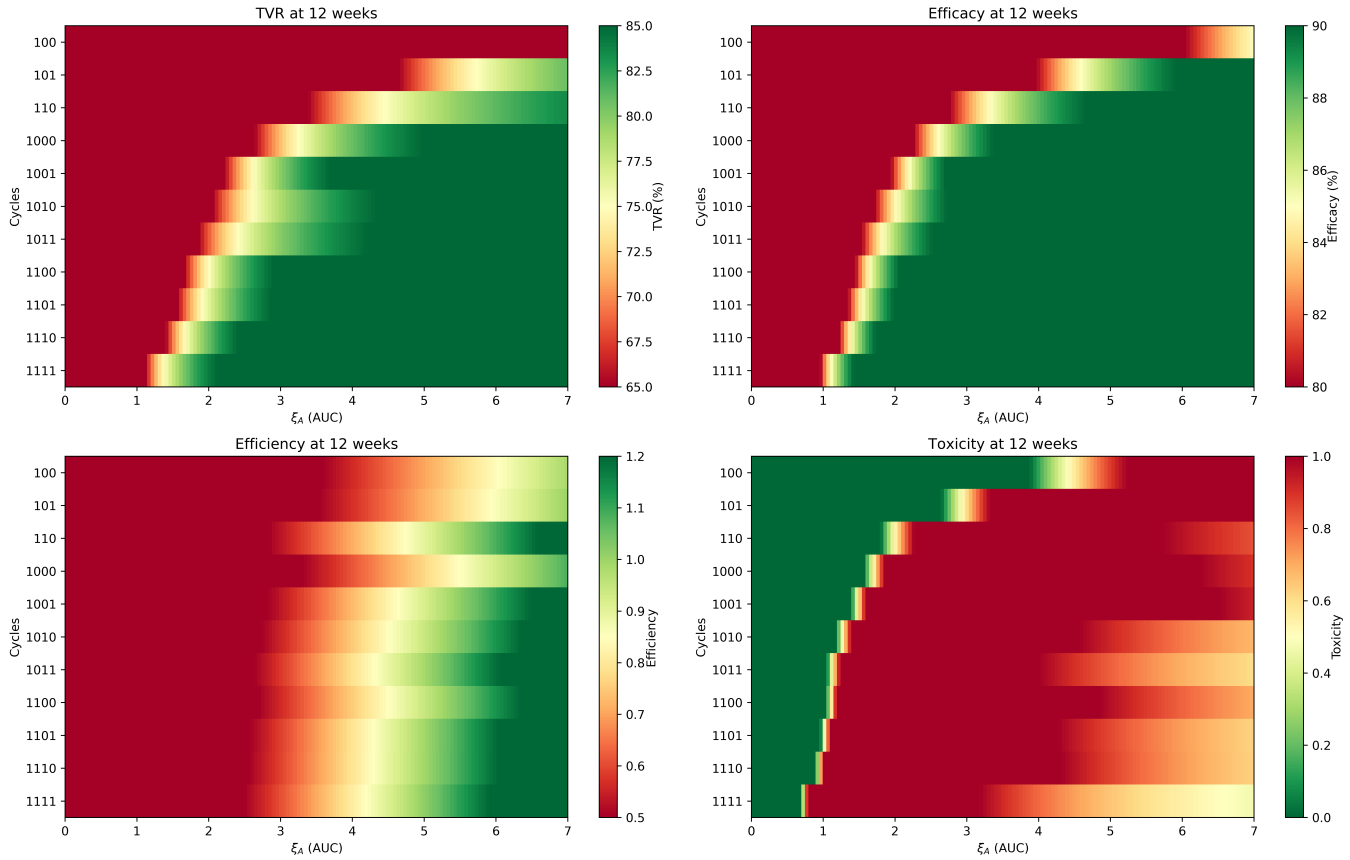

Figure 6: Heatmap of 21-day and 28-day cycles. The binary encodings on the y-axis correspond to infusion days 1, 8 and 15 for the 21-day cycles, and 1, 8, 15 and 21 for the 28-day cycles.

It is also difficult to compare our results to pre-existing clinical trials for first-line neoadjuvant HGSOC due to the lack of time-series data. However, we run the chemotherapy regimens from the clinical trials in Table 7 on our model and compare them with the SR and optimal weekly solutions in Table 8. We also display their TVR, efficacy, efficiency and toxicity in Figure 7.

Table 7: Neoadjuvant clinical trials with varying dosing regimens. Paclitaxel dose (P dose) is given in (mg/m^2), and carboplatin dose (A dose) is given in AUC. *Dose given on Day 1, 8, 15.

Trial	P **Dose**	**Freq.**	A **Dose**	**Freq.**	**Reference**
MITO-7	60	Weekly	2	Weekly	[160]
S B Dessai et. al/ICON8	80	Weekly	2	Weekly	[161, 162]
T. Safra et. al*	80	28-day cycle	2	28-day cycle	[161]
ICON8	80	Weekly	5	Triweekly	[162]
GOG-0262/JGOG3016	80	Weekly	6	Triweekly	[163, 164]

Table 8: Comparison of TVR, efficacy, efficiency and toxicity for various chemotherapy regimens.

Regimen	**TVR (%)**	**Efficacy (%)**	**Efficiency**	**Toxicity**
Standard Regimen	75.85	89.86	1.00	0.87
Optimal Weekly	75.83	89.86	1.92	0.28
MITO-7	86.36	94.27	0.87	0.41
S B Dessai et. al/ICON8	86.63	94.39	0.79	0.42
T. Safra et. al	84.59	93.53	0.79	0.41
ICON8	79.01	91.19	0.41	0.71
GOG-0262/JGOG3016	83.08	93.90	0.36	0.86

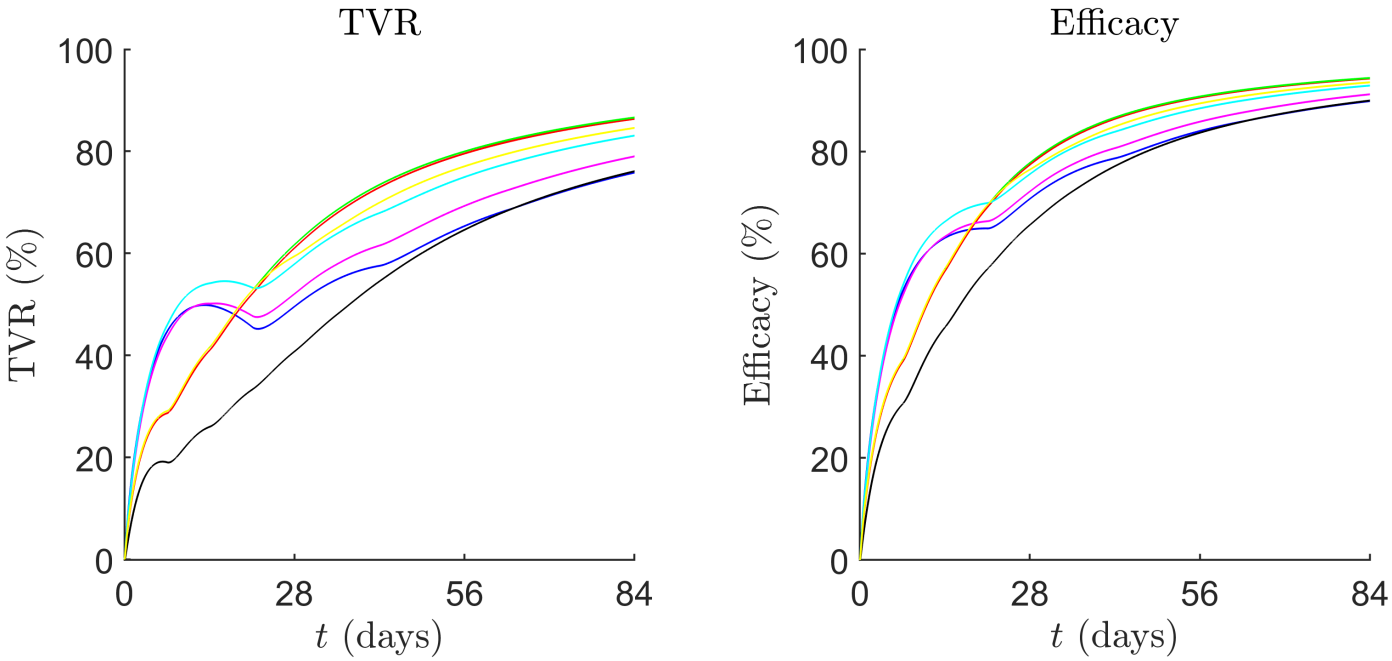

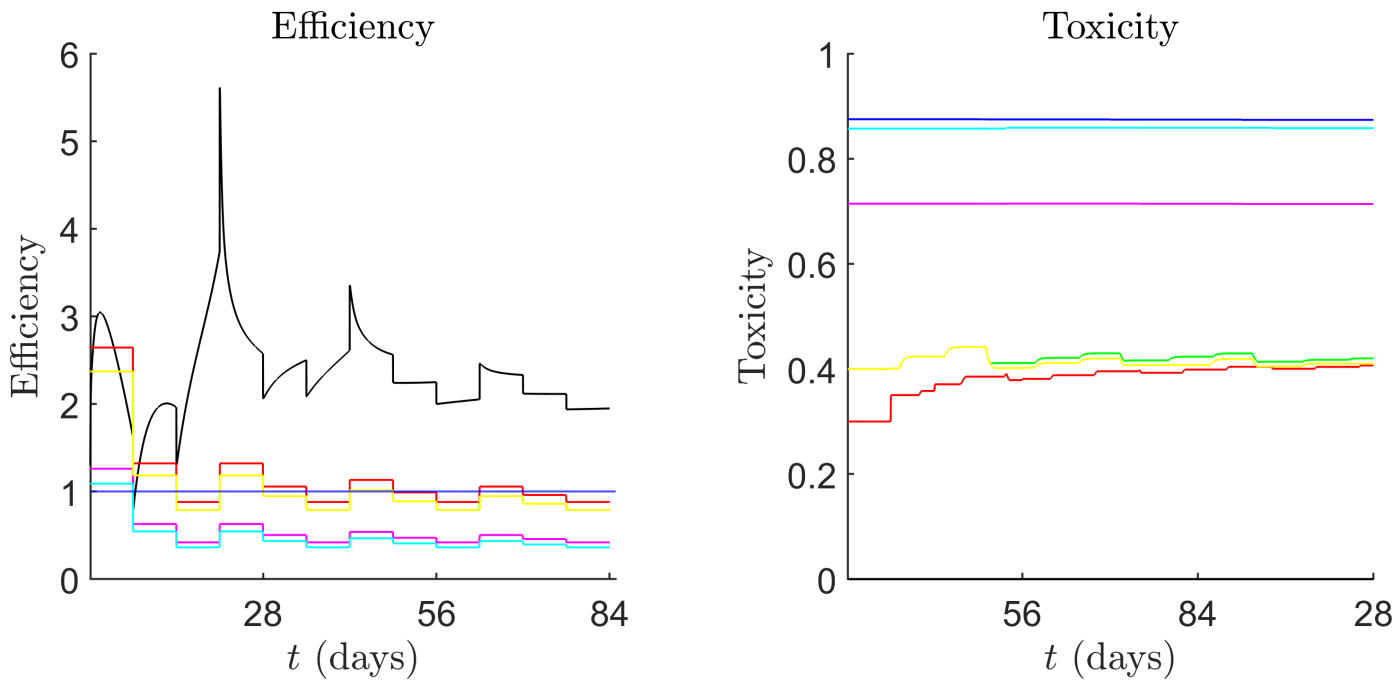

Figure 7: Time traces of TVR, efficacy, efficiency and toxicity. SR in blue, MITO-7 in red, S B Dessai et. al/ICON8 in green, T. Safra et. al in yellow, ICON8 trial in magenta, GOG-0262/JGOG3016 in cyan and the optimal weekly solution in black.

5 Discussion

To explain the behaviour of the treatment regimens, we first analyse the immune trajectories from Figure 4 to understand the TME in the absence of treatment. At first, we analyse the effects of paclitaxel and carboplatin treatment, by only considering the SR. One of the main drivers of the immune response against cancer is TNF and IFN-γ induced cancer cell necrosis, which triggers the release of DAMPs and the maturation of immature DCs. Elevated levels of TGF-β and IL-10 inhibit this maturation, causing decreased activation of CD8+ and Th1 cells in the TDLN which migrate to the TS and sustain the cytotoxic response. We observe on average elevated levels of TGF-β and IL-10 at 1.24×10^{-6} g/cm^3 and 7.70×10^{-7} g/cm^3, respectively, for no treatment, compared to 4.79×10^{-7} g/cm^3 and 1.07×10^{-7} g/cm^3 with treatment. As TGF-β promotes the proliferation of Tregs, we observe a relatively increased Treg population of 9.34×10^6 cell/cm^3 without treatment compared to 5.95×10^6 cell/cm^3 with treatment, which inhibits the cytotoxic activity of CD8+ T cells and Th1 cells at the TS. Tregs also secrete additional TGF-β and IL-10, promoting an immunosuppressive positive feed-forward loop. Additionally, as IL-10 and TGF-β drive macrophage polarisation toward the anti-inflammatory M2 phenotype, this establishes another immunosuppressive feed-forward loop as M2 macrophages secrete IL-10 and TGF-β. Hence, we observe an increased average M1/M2 ratio of 0.40 for the SR compared to 0.28 without treatment. This reinforces an environment where cytotoxic immune cells are functionally impaired and outnumbered by immunosuppressive components, allowing cancer to proliferate and overwhelm the immune system.

During chemotherapy treatment, the reduction in cancer concentration causes a large decrease in TGF-β and IL-10, which decreases the polarisation of macrophages to the M2 phenotype and the expansion of Tregs. As Tregs inhibit CD8+ and Th1 secretion of IL-2, a decreased Treg population reduces this inhibition, promoting a positive feedback loop, as IL-2 is a growth factor for CD8+ and Th1 cells.

At the same time, a reduced effector Treg population decreases the inhibition of IFN-γ production by CD8+ T cells and NK cells, which, in combination with increased IL-2 and decreased TGF-β and IL-10, leads to an increase in the polarisation and repolarisation of macrophages to the pro-inflammatory M1 phenotype. These macrophages further secrete pro-inflammatory cytokines, including IL-12, TNF and IFN-γ. However, the TNF concentration decreases to 2.04×10^{-10} g/cm^3 with treatment at 12 weeks compared to 2.28×10^{-10} g/cm^3 without treatment. This is due to a reduction in the DAMP concentration and the subsequent maturation of DCs, which leads to a decreased activation of T cells in the TDLN, and hence T cell populations at the TS relative to those without treatment. Additionally, chemotherapy, which targets proliferating cells such as T cells, further contributes to the decrease, leading to reduced secretion rates of cytokines such as TNF and IFN-γ as we assumed a constant influx of naïve immune cells over time. Hence, we observe that chemotherapy disrupts immunosuppressive feedback loops in the TME, allowing the immune system to shift towards a pro-inflammatory response.

Within the chemotherapy regimens, we find that lower dosage, more frequent carboplatin is more efficient and comparably as effective than higher dosages with lower frequencies (Table 6). In the absence of carboplatin resistance, we expect that optimal regimens feature carboplatin monotherapy, as carboplatin has a prolonged duration of cytotoxic activity than paclitaxel, despite having a shorter plasma half-life (1–2 hours vs 9.9 hours) [152, 153]. This is due to the behaviour of the platinum moiety, which, after hydrolysis, binds irreversibly to plasma proteins and is eliminated over several days [165]. As carboplatin is more cytotoxic per milligram than paclitaxel, the most efficient regimens that are both non-toxic and achieve an acceptable TVR do not include paclitaxel. High-frequency dosing of carboplatin results in decreased oscillation in carboplatin concentrations so that cancer cells are subjected to continuous cytotoxicity, inhibiting cancer growth between infusions, as observed in Figure 3 for the optimal triweekly regimen and SR. As shown in Figure 4, the optimal biweekly, weekly, 21-day, and 28-day cyclic regimens consistently sustain a non-zero carboplatin concentration, with each subsequent administration resulting in an increased sustained carboplatin concentration, whereas the corresponding concentrations for the optimal triweekly regimen and SR rapidly approach zero after one week. As the peak concentrations reduce even with lower dosing, these solutions exhibit a lower toxicity, with an average of 0.37 compared to the optimal triweekly regimen and SR with an average of 0.84.

Analysing the TVR can provide further insights into these results. The SR, despite its high toxicity, leads to the largest increase in TVR in the first two weeks. However, due to the longer rest periods required to tolerate this treatment, the TVR decreases due to cancer growth in the absence of sustained cytotoxicity from chemotherapy between cycles (Figure 5). The rates of growth also decrease as treatment progresses due to a lower cancer concentration and shift towards a more pro-inflammatory immune state in which cytotoxic cells and cytokines promote cancer lysis in between cycles. Although the TVR of the biweekly, weekly, 21-day and 28-day cyclic regimens have a less rapid increase in the early stages of treatment, they gradually increase and exhibit a smaller degree of growth between cycles due to more frequent infusions. We also observe that all optimal regimens are more efficient than the SR at all time points and vary according to infusion spacing and dosing. On the first day, the efficiency is inversely proportional to the dosages administered, with lower-dosage regimens displaying the highest efficiency due to similar TVRs between the regimens at the initial infusion. On days in which the SR regimen does not inject but the biweekly, weekly, or cyclic regimens do, we observe a sharp decrease in efficiency, followed by a gradual increase in efficiency due to the delay in the effects of chemotherapy in the system. For days on which all regimens include a dose coinciding with that of the SR infusion, we observe a spike in efficiency as the SR has a higher comparative drug concentration, with the magnitude of this spike decreasing as the drug concentrations over time become more similar. In combination with the similarity of the TVR time trace between regimens, this also explains the

reduction in oscillations as the treatment approaches 84 days since commencement.

Additionally, 21-day and 28-day cyclic regimens can serve as effective alternative dosing strategies comparable to those with constant spacing, with the inclusion of rest weeks allowing patients to recover from side effects, potentially improving treatment adherence. From Table 6, we observe that rest weeks are compensated by higher carboplatin doses compared to regimens administered weekly. We also observe in Figure 6 that within the 21-day and 28-day cyclic treatments, regimens that administer infusions in the first two weeks can sustain lower overall carboplatin dosages while maintaining comparable TVR, efficacy, and toxicity to the optimal biweekly and weekly regimens. Notably, dosing on days 1 and 8 in the 28-day cycle appears sufficient to sustain a one to two-week break, as indicated by the similar heatmap profiles of the 28-day cycles 1101 and 1100. However, when a break is introduced on day 8 (as in cycles 1011, 1010, 1001, and 1000), higher carboplatin doses are required to achieve a comparable TVR, efficacy, and toxicity profile to regimens that include dosing on day 8. This is due to the lack of sustained cytotoxic response in the early stages of treatment, allowing the still sizeable tumour to recover before the immune response becomes sufficiently pro-inflammatory. We also note that for all 21-day and 28-day cyclic regimens, except for the 21-day cycles 100 and 101 and the 28-day cycle 1000, which omit dosing on day 8, the efficacy profiles remain similar. Although the 28-day cycles 1011, 1010, and 1001 also omit dosing on day 8, they have a lower ratio of rest to non-rest weeks, suggesting that longer rest periods combined with later administration leads to an increase in tumour concentration, necessitating higher drug doses to compensate. This, in turn, reduces overall treatment efficiency, and as a result, the optimal 21-day and 28-day cyclic regimens administer infusions in the first two and three weeks, respectively.

Heatmaps of the triweekly, biweekly and weekly regimens, shown in Figure B.1, Figure B.2 and Figure B.3, respectively, compare the TVR, efficacy, efficiency and toxicity of treatments consisting of varying carboplatin and paclitaxel doses. Of note, is that the region of acceptable TVR shifts according to the infusion frequency of carboplatin, with higher frequencies enabling lower doses of carboplatin to sustain TVRs similar to those of lower frequencies. Compared to the SR, we observe in Figure B.1, that high TVRs for triweekly regimens only occur above 5.5 AUC, and so all effective triweekly regimens will exhibit a high toxicity. Efficiency also primarily depends on the frequency and dosage of administered carboplatin, with more frequent, low-dose carboplatin leading to higher efficiency. However, for the biweekly and weekly regimens, Figure B.2 and Figure B.3 demonstrate that the efficiency of treatments with paclitaxel doses below 80 mg/m^2 increases if sufficient carboplatin is administered. Interestingly, clinical trials comparing weekly paclitaxel (60 and 80 mg/m^2) to weekly carboplatin at 2 AUC have reported PFS comparable to the SR, but with reduced patient toxicity [29, 166, 167]. We observe in Table 8 and Figure 7 that the addition of paclitaxel increases the TVR compared to the optimal weekly solution, from 75.83% to 86.36% and 86.63% for 60 mg/m^2 and 80 mg/m^2, respectively, at the expense of increased toxicity. However, Figure B.3 indicates that dosages of paclitaxel beyond 85 mg/m^2 have a poorer efficiency and higher toxicity, and so, the optimal regimens will have a paclitaxel dose less than 85 mg/m^2. Due to the increased efficacy of carboplatin per milligram, compared to paclitaxel, the optimal treatments, which balance TVR, efficiency and toxicity, consist solely of carboplatin. In particular, these results demonstrate diminishing increases in TVR as chemotherapy dosing increases, which are accompanied by disproportionate increases in toxicity.

It should be noted that the model has several limitations, with the potential for addressing these issues serving as exciting avenues for future research.

- Although most OC patients exhibit an initial response to first-line chemotherapy and the in-

clusion of platinum agent is a dominant factor in the survival of ovarian cancer, in practice, combination chemotherapy with independent mechanisms of action is preferred to minimise the evolution of platinum resistance [5, 168–170]. Future work involves extending this model to incorporate resistance and optimise regimens to maintain effective cancer reduction whilst minimising the effects of acquired resistance.

- Our model does not account for spatial effects, which could provide insights into the distribution and clustering of immune cell populations within the TME and how these spatial dynamics influence tumour progression and treatment outcomes [171, 172].
- We considered only the M1/M2 macrophage dichotomy; however, their inherent plasticity suggests that their phenotypes are better represented as a continuum, allowing them to adopt mixed functional states that encompass both pro-inflammatory M1 and anti-inflammatory M2 characteristics [173].
- We did not account for the role of cytokines in the TDLN, which can influence T cell activation and proliferation and play a significant role in effector T cell differentiation [174, 175].

In this work, we have provided a framework for mathematically modelling the immunobiology of HGSOC using delay-differential equations. We analysed the optimised paclitaxel and carboplatin therapies for tumour volume reduction, efficacy, efficiency and toxicity for first-line chemotherapy treatment, and we conclude that low-dose high-frequency carboplatin monotherapy provides comparable results to the standard regimen. Additionally, 21-day and 28-day cyclic regimens can serve as alternative dosing strategies with rest weeks, allowing patients to recover from the toxic side effects of chemotherapy. Future work will focus on extending this model to incorporate carboplatin resistance, a major challenge in HGSOC, and optimising treatment to minimise its impact while maintaining effective tumour reduction.

6 CRediT authorship contribution statement

Cristina Koprinski: conceptualisation, data curation, formal analysis, funding acquisition, investigation, methodology, project administration, resources, software, validation, visualisation, writing — original draft, writing — review & editing.
Georgio Hawi: conceptualisation, data curation, formal analysis, funding acquisition, investigation, methodology, project administration, resources, software, validation, visualisation, writing — original draft, writing — review & editing.
Peter S. Kim: conceptualisation, formal analysis, investigation, methodology, project administration, resources, supervision, validation, visualisation, writing — original draft, writing — review & editing.
Cristina Koprinski and Georgio Hawi contributed equally to this work.

7 Declaration of Competing Interests

The authors declare that they have no known competing financial interests or personal relationships that could have appeared to influence the work reported in this paper.

8 Data availability

All data and procedures are available within the manuscript and its Supporting Information file.

9 Acknowledgements

This work was supported by an Australian Academy of Technological Sciences and Engineering Elevate Scholarship and an Australian Government Research Training Program Scholarship. PSK gratefully acknowledges support from the Australian Research Council Discovery Project (DP230100485).

References

[1] Chandra A, Pius C, Nabeel M, Nair M, Vishwanatha JK, Ahmad S, et al. Ovarian cancer: Current status and strategies for improving therapeutic outcomes. Cancer Medicine. 2019 Sep;8(16):7018–7031. Available from: https://doi.org/10.1002/cam4.2560.

[2] Torre LA, Trabert B, DeSantis CE, Miller KD, Samimi G, Runowicz CD, et al. Ovarian cancer statistics, 2018. CA: A Cancer Journal for Clinicians. 2018 May;68(4):284–296. Available from: https://doi.org/10.3322/caac.21456.

[3] Pignata S, C Cecere S, Du Bois A, Harter P, Heitz F. Treatment of recurrent ovarian cancer. Annals of Oncology. 2017 Nov;28:viii51–viii56. Available from: https://doi.org/10.1093/annonc/mdx441.

[4] Liberto JM, Chen SY, Shih IM, Wang TH, Wang TL, Pisanic TR. Current and Emerging Methods for Ovarian Cancer Screening and Diagnostics: A Comprehensive Review. Cancers. 2022 Jun;14(12):2885. Available from: https://doi.org/10.3390/cancers14122885.

[5] St Laurent J, Liu JF. Treatment Approaches for Platinum-Resistant Ovarian Cancer. Journal of Clinical Oncology. 2024 Jan;42(2):127–133. Available from: https://doi.org/10.1200/JCO.23.01771.

[6] Duska LR, Tew WP, Moore KN. Epithelial Ovarian Cancer in Older Women: Defining the Best Management Approach. American Society of Clinical Oncology Educational Book. 2015 May;(35):e311–e321. Available from: https://doi.org/10.14694/EdBook_AM.2015.35.e311.

[7] Matulonis UA, Sood AK, Fallowfield L, Howitt BE, Sehouli J, Karlan BY. Ovarian cancer. Nature Reviews Disease Primers. 2016 Aug;2(1). Available from: https://doi.org/10.1038/nrdp.2016.61.

[8] Chang SJ, Hodeib M, Chang J, Bristow RE. Survival impact of complete cytoreduction to no gross residual disease for advanced-stage ovarian cancer: A meta-analysis. Gynecologic Oncology. 2013 Sep;130(3):493–498. Available from: https://doi.org/10.1016/j.ygyno.2013.05.040.

[9] Vergote I, Tropé CG, Amant F, Kristensen GB, Ehlen T, Johnson N, et al. Neoadjuvant Chemotherapy or Primary Surgery in Stage IIIC or IV Ovarian Cancer. New England Journal of Medicine. 2010 Sep;363(10):943–953. Available from: https://doi.org/10.1056/NEJMoa0908806.

[10] Kehoe S, Hook J, Nankivell M, Jayson GC, Kitchener H, Lopes T, et al. Primary chemotherapy versus primary surgery for newly diagnosed advanced ovarian cancer (CHORUS): an open-label, randomised, controlled, non-inferiority trial. The Lancet. 2015 Jul;386(9990):249–257. Available from: https://doi.org/10.1016/S0140-6736(14)62223-6.

[11] Onda T, Satoh T, Saito T, Kasamatsu T, Nakanishi T, Nakamura K, et al. Comparison of treatment invasiveness between upfront debulking surgery versus interval debulking surgery following neoadjuvant chemotherapy for stage III/IV ovarian, tubal, and peritoneal cancers in a phase III randomised trial: Japan Clinical Oncology Group Study JCOG0602. European Journal of Cancer. 2016 Sep;64:22–31. Available from: https://doi.org/10.1016/j.ejca.2016.05.017.

[12] Fagotti A, Ferrandina MG, Vizzielli G, Pasciuto T, Fanfani F, Gallotta V, et al. Randomized trial of primary debulking surgery versus neoadjuvant chemotherapy for advanced epithelial ovarian cancer (SCORPION-NCT01461850). International Journal of Gynecologic Cancer. 2020 Oct;30(11):1657–1664. Available from: https://doi.org/10.1136/ijgc-2020-001640.

[13] Nikolaidi A, Fountzilas E, Fostira F, Psyrri A, Gogas H, Papadimitriou C. Neoadjuvant treatment in ovarian cancer: New perspectives, new challenges. Frontiers in Oncology. 2022 Jul;12. Available from: https://doi.org/10.3389/fonc.2022.820128.

[14] Vergote I, Coens C, Nankivell M, Kristensen GB, Parmar MKB, Ehlen T, et al. Neoadjuvant chemotherapy versus debulking surgery in advanced tubo-ovarian cancers: pooled analysis of individual patient data from the EORTC 55971 and CHORUS trials. The Lancet Oncology. 2018 Dec;19(12):1680–1687. Available from: https://doi.org/10.1016/S1470-2045(18)30566-7.

[15] Vergote I, Gonzalez-Martin A, Lorusso D, Gourley C, Mirza MR, Kurtz JE, et al. Clinical research in ovarian cancer: consensus recommendations from the Gynecologic Cancer InterGroup. The Lancet Oncology. 2022 Aug;23(8):e374–e384. Available from: https://doi.org/10.1016/S1470-2045(22)00139-5.

[16] du Bois A, Quinn M, Thigpen T, Vermorken J, Avall-Lundqvist E, Bookman M, et al. 2004 consensus statements on the management of ovarian cancer: final document of the 3rd International Gynecologic Cancer Intergroup Ovarian Cancer Consensus Conference (GCIG OCCC 2004). Annals of Oncology. 2005;16:viii7–viii12. Available from: https://doi.org/10.1093/annonc/mdi961.

[17] González-Martín A, Sánchez-Lorenzo L, Bratos R, Márquez R, Chiva L. First-Line and Maintenance Therapy for Ovarian Cancer: Current Status and Future Directions. Drugs. 2014 May;74(8):879–889. Available from: https://doi.org/10.1007/s40265-014-0221-9.

[18] McGuire WP, Hoskins WJ, Brady MF, Kucera PR, Partridge EE, Look KY, et al. Cyclophosphamide and Cisplatin Compared with Paclitaxel and Cisplatin in Patients with Stage III and Stage IV Ovarian Cancer. New England Journal of Medicine. 1996 Jan;334(1):1–6. Available from: https://doi.org/10.1056/NEJM199601043340101.

[19] Piccart MJ. Randomized Intergroup Trial of Cisplatin-Paclitaxel Versus Cisplatin-Cyclophosphamide in Women With Advanced Epithelial Ovarian Cancer: Three-Year Results. Journal of the National Cancer Institute. 2000 May;92(9):699–708. Available from: https://doi.org/10.1093/jnci/92.9.699.

[20] Neijt JP, Engelholm SA, Tuxen MK, Sørensen PG, Hansen M, Sessa C, et al. Exploratory Phase III Study of Paclitaxel and Cisplatin Versus Paclitaxel and Carboplatin in Advanced Ovarian Cancer. Journal of Clinical Oncology. 2000 Sep;18(17):3084–3092. Available from: https://doi.org/10.1200/JCO.2000.18.17.3084.

[21] du Bois A. A Randomized Clinical Trial of Cisplatin/Paclitaxel Versus Carboplatin/Paclitaxel as First-Line Treatment of Ovarian Cancer. CancerSpectrum Knowledge Environment. 2003 Sep;95(17):1320–1329. Available from: https://doi.org/10.1093/jnci/djg036.

[22] McGuire WP, Markman M. Primary ovarian cancer chemotherapy: current standards of care. British Journal of Cancer. 2003 Dec;89(S3):S3–S8. Available from: https://doi.org/10.1038/sj.bjc.6601494.

[23] Gynecologic Oncology Group (Tokai G T, Kuzuya K, Ishikawa H, Kikkawa F, Nawa A, Fujimura H, et al. Optimal doses of paclitaxel and carboplatin combination chemotherapy for ovarian cancer: a phase I modified continual reassessment method study. International Journal of Clinical Oncology. 2001 Dec;6(6):271–278. Available from: https://doi.org/10.1007/s10147-001-8027-7.

[24] Basar OY, Mohammed S, Qoronfleh MW, Acar A. Optimizing cancer therapy: a review of the multifaceted effects of metronomic chemotherapy. Frontiers in Cell and Developmental Biology. 2024 May;12. Available from: https://doi.org/10.3389/fcell.2024.1369597.

[25] Pasquier E, Kavallaris M, André N. Metronomic chemotherapy: new rationale for new directions. Nature Reviews Clinical Oncology. 2010 Jun;7(8):455–465. Available from: https://doi.org/10.1038/nrclinonc.2010.82.

[26] Katsumata N, Yasuda M, Takahashi F, Isonishi S, Jobo T, Aoki D, et al. Dose-dense paclitaxel once a week in combination with carboplatin every 3 weeks for advanced ovarian cancer: a phase 3, open-label, randomised controlled trial. The Lancet. 2009 Oct;374(9698):1331–1338. Available from: https://doi.org/10.1016/S0140-6736(09)61157-0.

[27] Chan JK, Brady MF, Penson RT, Huang H, Birrer MJ, Walker JL, et al. Weekly vs. Every-3-Week Paclitaxel and Carboplatin for Ovarian Cancer. New England Journal of Medicine. 2016 Feb;374(8):738–748. Available from: https://doi.org/10.1056/NEJMoa1505067.

[28] Pignata S, Breda E, Scambia G, Pisano C, Zagonel V, Lorusso D, et al. A phase II study of weekly carboplatin and paclitaxel as first-line treatment of elderly patients with advanced ovarian cancer. Critical Reviews in Oncology/Hematology. 2008 Jun;66(3):229–236. Available from: https://doi.org/10.1016/j.critrevonc.2007.12.005.

[29] Pignata S, Scambia G, Katsaros D, Gallo C, Pujade-Lauraine E, De Placido S, et al. Carboplatin plus paclitaxel once a week versus every 3 weeks in patients with advanced ovarian cancer (MITO-7): a randomised, multicentre, open-label, phase 3 trial. The Lancet Oncology. 2014 Apr;15(4):396–405. Available from: https://doi.org/10.1016/S1470-2045(14)70049-X.

[30] Clamp AR, James EC, McNeish IA, Dean A, Kim JW, O'Donnell DM, et al. Weekly dose-dense chemotherapy in first-line epithelial ovarian, fallopian tube, or primary peritoneal carcinoma treatment (ICON8): primary progression free survival analysis results from a GCIG phase 3 randomised controlled trial. The Lancet. 2019 Dec;394(10214):2084–2095. Available from: https://doi.org/10.1016/S0140-6736(19)32259-7.

[31] Gong W, Yu R, Cao C, Fang Y, Zhao X, Gao Q. Dose-dense regimen versus conventional three-weekly paclitaxel combination with carboplatin chemotherapy in first-line ovarian cancer treatment: a systematic review and meta-analysis. Journal of Ovarian Research. 2023 Jul;16(1). Available from: https://doi.org/10.1186/s13048-023-01216-z.

[32] Lai X, Friedman A. Mathematical modeling in scheduling cancer treatment with combination of VEGF inhibitor and chemotherapy drugs. Journal of Theoretical Biology. 2019 Feb;462:490–498. Available from: https://doi.org/10.1016/j.jtbi.2018.11.018.

[33] Louzoun Y, Xue C, Lesinski GB, Friedman A. A mathematical model for pancreatic cancer growth and treatments. Journal of Theoretical Biology. 2014 Jun;351:74–82. Available from: https://doi.org/10.1016/j.jtbi.2014.02.028.

[34] dePillis L. Mathematical Model of Colorectal Cancer with Monoclonal Antibody Treatments. British Journal of Medicine and Medical Research. 2014 Jan;4(16):3101–3131. Available from: https://doi.org/10.9734/BJMMR/2014/8393.

[35] Sancho-Araiz A, Mangas-Sanjuan V, Trocóniz IF. The Role of Mathematical Models in Immuno-Oncology: Challenges and Future Perspectives. Pharmaceutics. 2021 Jul;13(7):1016. Available from: https://doi.org/10.3390/pharmaceutics13071016.

[36] Hawi G, Kim PS, Lee PP. Optimisation of neoadjuvant pembrolizumab therapy for locally advanced MSI-H/dMMR colorectal cancer using data-driven delay integro-differential equations. arXiv; 2024. arXiv:2411.12123 [q-bio.CB]. Available from: https://arxiv.org/abs/2411.12123.

[37] Hawi G, Kim PS, Lee PP. Optimisation of pembrolizumab therapy for de novo metastatic MSI-H/dMMR colorectal cancer using data-driven delay integro-differential equations. bioRxiv. 2025. Available from: https://www.biorxiv.org/content/early/2025/05/24/2025.05.23.655752.

[38] Panetta JC. A mathematical model of breast and ovarian cancer treated with paclitaxel. Mathematical Biosciences. 1997 Dec;146(2):89–113. Available from: https://doi.org/10.1016/S0025-5564(97)00077-1.

[39] Kohandel M, Sivaloganathan S, Oza A. Mathematical modeling of ovarian cancer treatments: Sequencing of surgery and chemotherapy. Journal of Theoretical Biology. 2006 Sep;242(1):62–68. Available from: https://doi.org/10.1016/j.jtbi.2006.02.001.

[40] Yan L, Wang J, Cai X, Liou Y, Shen H, Hao J, et al. Macrophage plasticity: signaling pathways, tissue repair, and regeneration. MedComm. 2024 Aug;5(8). Available from: https://doi.org/10.1002/mco2.658.

[41] Hernandez C, Huebener P, Schwabe RF. Damage-associated molecular patterns in cancer: a double-edged sword. Oncogene. 2016 Apr;35(46):5931–5941. Available from: https://doi.org/10.1038/onc.2016.104.

[42] Tiberio L, Del Prete A, Schioppa T, Sozio F, Bosisio D, Sozzani S. Chemokine and chemotactic signals in dendritic cell migration. Cellular; Molecular Immunology. 2018 Mar;15(4):346–352. Available from: https://doi.org/10.1038/s41423-018-0005-3.

[43] Bousso P. T-cell activation by dendritic cells in the lymph node: lessons from the movies. Nature Reviews Immunology. 2008 Sep;8(9):675–684. Available from: https://doi.org/10.1038/nri2379.

[44] Curtsinger JM, Johnson CM, Mescher MF. CD8 T Cell Clonal Expansion and Development of Effector Function Require Prolonged Exposure to Antigen, Costimulation, and Signal 3 Cytokine. The Journal of Immunology. 2003 Nov;171(10):5165–5171. Available from: https://doi.org/10.4049/jimmunol.171.10.5165.

[45] Smith KA. Interleukin-2: Inception, Impact, and Implications. Science. 1988 May;240(4856):1169–1176. Available from: https://doi.org/10.1126/science.3131876.

[46] Hwang ES, Hong JH, Glimcher LH. IL-2 production in developing Th1 cells is regulated by heterodimerization of RelA and T-bet and requires T-bet serine residue 508. The Journal of Experimental Medicine. 2005 Nov;202(9):1289–1300. Available from: https://doi.org/10.1084/jem.20051044.

[47] Trinchieri G. Interleukin-12 and the regulation of innate resistance and adaptive immunity. Nature Reviews Immunology. 2003 Feb;3(2):133–146. Available from: https://doi.org/10.1038/nri1001.

[48] Wu C, Xue Y, Wang P, Lin L, Liu Q, Li N, et al. IFN-γ Primes Macrophage Activation by Increasing Phosphatase and Tensin Homolog via Downregulation of miR-3473b. The Journal of Immunology. 2014 Sep;193(6):3036–3044. Available from: https://doi.org/10.4049/jimmunol.1302379.

[49] Jorgovanovic D, Song M, Wang L, Zhang Y. Roles of IFN-γ in tumor progression and regression: a review. Biomarker Research. 2020 Sep;8(1). Available from: https://doi.org/10.1186/s40364-020-00228-x.

[50] Sousa GFd, Wlodarczyk SR, Monteiro G. Carboplatin: molecular mechanisms of action associated with chemoresistance. Brazilian Journal of Pharmaceutical Sciences. 2014 Dec;50(4):693–701. Available from: https://doi.org/10.1590/S1984-82502014000400004.

[51] Coleman SC, Stewart ZA, Day TA, Netterville JL, Burkey BB, Pietenpol JA. Analysis of Cell-Cycle Checkpoint Pathways in Head and Neck Cancer Cell Lines. Archives of Otolaryngology–Head; Neck Surgery. 2002 Feb;128(2):167. Available from: https://doi.org/10.1001/archotol.128.2.167.

[52] Weaver BA. How Taxol/paclitaxel kills cancer cells. Molecular Biology of the Cell. 2014 Sep;25(18):2677–2681. Available from: https://doi.org/10.1091/mbc.E14-04-0916.

[53] Khing TM, Choi WS, Kim DM, Po WW, Thein W, Shin CY, et al. The effect of paclitaxel on apoptosis, autophagy and mitotic catastrophe in AGS cells. Scientific Reports. 2021 Dec;11(1). Available from: https://doi.org/10.1038/s41598-021-02503-9.

[54] Thomas DA, Massagué J. TGF-β directly targets cytotoxic T cell functions during tumor evasion of immune surveillance. Cancer Cell. 2005 Nov;8(5):369–380. Available from: https://doi.org/10.1016/j.ccr.2005.10.012.

[55] Rich S, Seelig M, Lee HM, Lin J. Transforming growth factor beta 1 costimulated growth and regulatory function of staphylococcal enterotoxin B-responsive CD8+ T cells. Journal of immunology (Baltimore, Md: 1950). 1995;155(2):609-18.

[56] Cachot A, Bilous M, Liu YC, Li X, Saillard M, Cenerenti M, et al. Tumor-specific cytolytic CD4 T cells mediate immunity against human cancer. Science Advances. 2021 Feb;7(9). Available from: https://doi.org/10.1126/sciadv.abe3348.

[57] Carlsten M, Björkström NK, Norell H, Bryceson Y, van Hall T, Baumann BC, et al. DNAX Accessory Molecule-1 Mediated Recognition of Freshly Isolated Ovarian Carcinoma by Resting Natural Killer Cells. Cancer Research. 2007 Feb;67(3):1317–1325. Available from: https://doi.org/10.1158/0008-5472.CAN-06-2264.

[58] Geller MA, Knorr DA, Hermanson DA, Pribyl L, Bendzick L, Mccullar V, et al. Intraperitoneal delivery of human natural killer cells for treatment of ovarian cancer in a mouse xenograft model. Cytotherapy. 2013 Oct;15(10):1297–1306. Available from: https://doi.org/10.1016/j.jcyt.2013.05.022.

[59] Li C, Jiang P, Wei S, Xu X, Wang J. Regulatory T cells in tumor microenvironment: new mechanisms, potential therapeutic strategies and future prospects. Molecular Cancer. 2020 Jul;19(1). Available from: https://doi.org/10.1186/s12943-020-01234-1.

[60] Saleh R, Elkord E. FoxP3+ T regulatory cells in cancer: Prognostic biomarkers and therapeutic targets. Cancer Letters. 2020 Oct;490:174–185. Available from: https://doi.org/10.1016/j.canlet.2020.07.022.

[61] Takeuchi Y, Nishikawa H. Roles of regulatory T cells in cancer immunity. International Immunology. 2016 May;28(8):401–409. Available from: https://doi.org/10.1093/intimm/dxw025.

[62] Viel S, Marçais A, Guimaraes FSF, Loftus R, Rabilloud J, Grau M, et al. TGF-β Inhibits the Activation and Functions of NK Cells by Repressing the mTOR Pathway. Science Signaling. 2016 Feb;9(415). Available from: http://doi.org/10.1126/scisignal.aad1884.

[63] Gong Y, Fan Z, Luo G, Yang C, Huang Q, Fan K, et al. The role of necroptosis in cancer biology and therapy. Molecular Cancer. 2019 May;18(1). Available from: https://doi.org/10.1186/s12943-019-1029-8.

[64] McCabe KE, Bacos K, Lu D, Delaney JR, Axelrod J, Potter MD, et al. Triggering necroptosis in cisplatin and IAP antagonist-resistant ovarian carcinoma. Cell Death; Disease. 2014 Oct;5(10):e1496–e1496. Available from: https://doi.org/10.1038/cddis.2014.448.

[65] Balachandran S, Adams GP. Interferon-γ-Induced Necrosis: An Antitumor Biotherapeutic Perspective. Journal of Interferon; Cytokine Research. 2013 Apr;33(4):171–180. Available from: https://doi.org/10.1089/jir.2012.0087.

[66] Murao A, Aziz M, Wang H, Brenner M, Wang P. Release mechanisms of major DAMPs. Apoptosis. 2021 Mar;26(3–4):152–162. Available from: https://doi.org/10.1007/s10495-021-01663-3.

[67] Chrisikos TT, Zhou Y, Slone N, Babcock R, Watowich SS, Li HS. Molecular regulation of dendritic cell development and function in homeostasis, inflammation, and cancer. Molecular Immunology. 2019 Jun;110:24–39. Available from: https://doi.org/10.1016/j.molimm.2018.01.014.

[68] Morel A, Quaratino S, Douek DC, Londei M. Split activity of interleukin-10 on antigen capture and antigen presentation by human dendritic cells: Definition of a maturative step. European Journal of Immunology. 1997 Jan;27(1):26–34. Available from: https://doi.org/10.1002/eji.1830270105.

[69] Lanzavecchia A, Sallusto F. Regulation of T Cell Immunity by Dendritic Cells. Cell. 2001 Aug;106(3):263–266. Available from: https://doi.org/10.1016/S0092-8674(01)00455-X.

[70] Wei S, Kryczek I, Zou W. Regulatory T-cell compartmentalization and trafficking. Blood. 2006 Jul;108(2):426–431. Available from: https://doi.org/10.1182/blood-2006-01-0177.

[71] McNally A, Hill GR, Sparwasser T, Thomas R, Steptoe RJ. CD4+ CD25+ regulatory T cells control CD8+ T-cell effector differentiation by modulating IL-2 homeostasis. Proceedings of the National Academy of Sciences. 2011 Apr;108(18):7529–7534. Available from: https://doi.org/10.1073/pnas.1103782108.

[72] Trandem K, Anghelina D, Zhao J, Perlman S. Regulatory T Cells Inhibit T Cell Proliferation and Decrease Demyelination in Mice Chronically Infected with a Coronavirus. The Journal of Immunology. 2010 Apr;184(8):4391–4400. Available from: https://doi.org/10.4049/jimmunol.0903918.

[73] Chaput N, Darrasse-Jèze G, Bergot AS, Cordier C, Ngo-Abdalla S, Klatzmann D, et al. Regulatory T Cells Prevent CD8 T Cell Maturation by Inhibiting CD4 Th Cells at Tumor Sites. The Journal of Immunology. 2007 Oct;179(8):4969–4978. Available from: https://doi.org/10.4049/jimmunol.179.8.4969.

[74] Groux H, Bigler M, de Vries JE, Roncarolo MG. Inhibitory and Stimulatory Effects of IL-10 on Human CD8+ T Cells. The Journal of Immunology. 1998 Apr;160(7):3188–3193. Available from: https://doi.org/10.4049/jimmunol.160.7.3188.

[75] Abbas AK, Murphy KM, Sher A. Functional diversity of helper T lymphocytes. Nature. 1996 Oct;383(6603):787–793. Available from: https://doi.org/10.1038/383787a0.

[76] Chen L, Grabowski KA, Xin Jp, Coleman J, Huang Z, Espiritu B, et al. IL-4 Induces Differentiation and Expansion of Th2 Cytokine-Producing Eosinophils. The Journal of Immunology. 2004 Feb;172(4):2059–2066. Available from: https://doi.org/10.4049/jimmunol.172.4.2059.

[77] Silva SL, Albuquerque AS, Serra-Caetano A, Foxall RB, Pires AR, Matoso P, et al. Human naïve regulatory T-cells feature high steady-state turnover and are maintained by IL-7. Oncotarget. 2016 Feb;7(11):12163–12175. Available from: https://doi.org/10.18632/oncotarget.7512.

[78] Zheng SG, Wang J, Wang P, Gray JD, Horwitz DA. IL-2 Is Essential for TGF-β to Convert Naive CD4+CD25- Cells to CD25+Foxp3+ Regulatory T Cells and for Expansion of These Cells. The Journal of Immunology. 2007 Feb;178(4):2018–2027. Available from: https://doi.org/10.4049/jimmunol.178.4.2018.

[79] Luque-Martin R, Angell DC, Kalxdorf M, Bernard S, Thompson W, Eberl HC, et al. IFN-γ Drives Human Monocyte Differentiation into Highly Proinflammatory Macrophages That Resemble a Phenotype Relevant to Psoriasis. The Journal of Immunology. 2021 Jul;207(2):555–568. Available from: https://doi.org/10.4049/jimmunol.2001310.

[80] Mosser DM, Edwards JP. Exploring the full spectrum of macrophage activation. Nature Reviews Immunology. 2008 Dec;8(12):958–969. Available from: https://doi.org/10.1038/nri2448.

[81] Fairweather D, Cihakova D. Alternatively activated macrophages in infection and autoimmunity. Journal of Autoimmunity. 2009 Nov;33(3–4):222–230. Available from: https://doi.org/10.1016/j.jaut.2009.09.012.

[82] Chen S, Saeed AFUH, Liu Q, Jiang Q, Xu H, Xiao GG, et al. Macrophages in immunoregulation and therapeutics. Signal Transduction and Targeted Therapy. 2023 May;8(1). Available from: https://doi.org/10.1038/s41392-023-01452-1.

[83] Wu X, Xu W, Feng X, He Y, Liu X, Gao Y, et al. TNF-a mediated inflammatory macrophage polarization contributes to the pathogenesis of steroid-induced osteonecrosis in mice. International Journal of Immunopathology and Pharmacology. 2015 Jul;28(3):351–361. Available from: https://doi.org/10.1177/0394632015593228.

[84] Zhang F, Wang H, Wang X, Jiang G, Liu H, Zhang G, et al. TGF-β induces M2-like macrophage polarization via SNAIL-mediated suppression of a pro-inflammatory phenotype. Oncotarget. 2016 Jul;7(32):52294–52306. Available from: https://doi.org/10.18632/oncotarget.10561.

[85] Trinchieri G. In: Biology of Natural Killer Cells. Elsevier; 1989. p. 187–376. Available from: https://doi.org/10.1016/S0065-2776(08)60664-1.

[86] Zwirner NW, Ziblat A. Regulation of NK Cell Activation and Effector Functions by the IL-12 Family of Cytokines: The Case of IL-27. Frontiers in Immunology. 2017 Jan;8. Available from: https://doi.org/10.3389/fimmu.2017.00025.

[87] Walzer T, Dalod M, Robbins SH, Zitvogel L, Vivier E. Natural-killer cells and dendritic cells: "l'union fait la force". Blood. 2005 Oct;106(7):2252–2258. Available from: https://doi.org/10.1182/blood-2005-03-1154.

[88] Kalia V, Sarkar S. Regulation of Effector and Memory CD8 T Cell Differentiation by IL-2—A Balancing Act. Frontiers in Immunology. 2018 Dec;9. Available from: https://doi.org/10.3389/fimmu.2018.02987.

[89] Tsyklauri O, Chadimova T, Niederlova V, Kovarova J, Michalik J, Malatova I, et al. Regulatory T cells suppress the formation of potent KLRK1 and IL-7R expressing effector CD8 T cells by limiting IL-2. eLife. 2023 Jan;12. Available from: https://doi.org/10.7554/eLife.79342.

[90] O'Garra A, Vieira PL, Vieira P, Goldfeld AE. IL-10–producing and naturally occurring CD4+ Tregs: limiting collateral damage. Journal of Clinical Investigation. 2004 Nov;114(10):1372–1378. Available from: https://doi.org/10.1172/JCI23215.

[91] Schweer D, McAtee A, Neupane K, Richards C, Ueland F, Kolesar J. Tumor-Associated Macrophages and Ovarian Cancer: Implications for Therapy. Cancers. 2022 Apr;14(9):2220. Available from: https://doi.org/10.3390/cancers14092220.

[92] Zhou J, Ye F, Chen H, Lv W, Gan N. The Expression of Interleukin-10 in Patients with Primary Ovarian Epithelial Carcinoma and in Ovarian Carcinoma Cell Lines. Journal of International Medical Research. 2007 May;35(3):290–300. Available from: https://doi.org/10.1177/147323000703500302.

[93] Pan J, Zhang M, Wang J, Wang Q, Xia D, Sun W, et al. Interferon-γ is an autocrine mediator for dendritic cell maturation. Immunology Letters. 2004 Jun;94(1–2):141–151. Available from: https://doi.org/10.1016/j.imlet.2004.05.003.

[94] Jensen SS, Gad M. Differential induction of inflammatory cytokines by dendritic cells treated with novel TLR-agonist and cytokine based cocktails: targeting dendritic cells in autoimmunity. Journal of Inflammation. 2010;7(1):37. Available from: https://doi.org/10.1186/1476-9255-7-37.

[95] Ma X, Yan W, Zheng H, Du Q, Zhang L, Ban Y, et al. Regulation of IL-10 and IL-12 production and function in macrophages and dendritic cells. F1000Research. 2015 Dec;4:1465. Available from: https://doi.org/10.12688/f1000research.7010.1.

[96] Kennedy R, Celis E. Multiple roles for CD4+ T cells in anti-tumor immune responses. Immunological Reviews. 2008 Mar;222(1):129–144. Available from: https://doi.org/10.1111/j.1600-065X.2008.00616.x.

[97] Liu T, Li Y, Wang X, Yang X, Fu Y, Zheng Y, et al. The role of interferons in ovarian cancer progression: Hinderer or promoter? Frontiers in Immunology. 2022 Dec;13. Available from: https://doi.org/10.3389/fimmu.2022.1087620.

[98] Panduro M, Benoist C, Mathis D. T reg cells limit IFN-γ production to control macrophage accrual and phenotype during skeletal muscle regeneration. Proceedings of the National Academy of Sciences. 2018 Feb;115(11). Available from: https://doi.org/10.1073/pnas.1800618115.

[99] Tau GZ, Cowan SN, Weisburg J, Braunstein NS, Rothman PB. Regulation of IFN-γ Signaling Is Essential for the Cytotoxic Activity of CD8+ T Cells. The Journal of Immunology. 2001 Nov;167(10):5574–5582. Available from: https://doi.org/10.4049/jimmunol.167.10.5574.

[100] Chun N, Ang RL, Chan M, Fairchild RL, Baldwin WM, Horwitz JK, et al. T cell–derived tumor necrosis factor induces cytotoxicity by activating RIPK1-dependent target cell death. JCI Insight. 2021 Dec;6(24). Available from: https://doi.org/10.1172/jci.insight.148643.

[101] Fauriat C, Long EO, Ljunggren HG, Bryceson YT. Regulation of human NK-cell cytokine and chemokine production by target cell recognition. Blood. 2010 Mar;115(11):2167–2176. Available from: https://doi.org/10.1182/blood-2009-08-238469.

[102] Chen W, Wahl SM. TGF-β: the missing link in CD4+CD25+ regulatory T cell-mediated immunosuppression. Cytokine; Growth Factor Reviews. 2003 Apr;14(2):85–89. Available from: https://doi.org/10.1016/S1359-6101(03)00003-0.

[103] Roane BM, Meza-Perez S, Katre AA, Goldsberry WN, Randall TD, Norian LA, et al. Neutralization of TGF-β Improves Tumor Immunity and Reduces Tumor Progression in Ovarian Carcinoma. Molecular Cancer Therapeutics. 2021 Mar;20(3):602–611. Available from: https://doi.org/10.1158/1535-7163.MCT-20-0412.

[104] Haque S, Morris JC. Transforming growth factor-β: A therapeutic target for cancer. Human Vaccines; Immunotherapeutics. 2017 Jun;13(8):1741–1750. Available from: https://doi.org/10.1080/21645515.2017.1327107.

[105] Truxova I, Cibula D, Spisek R, Fucikova J. Targeting tumor-associated macrophages for successful immunotherapy of ovarian carcinoma. Journal for ImmunoTherapy of Cancer. 2023 Feb;11(2):e005968. Available from: https://doi.org/10.1136/jitc-2022-005968.

[106] Snowden TJ, van der Graaf PH, Tindall MJ. Methods of Model Reduction for Large-Scale Biological Systems: A Survey of Current Methods and Trends. Bulletin of Mathematical Biology. 2017 Jun;79(7):1449-86. Available from: https://doi.org/10.1007/s11538-017-0277-2.

[107] Cui A, Huang T, Li S, Ma A, Pérez JL, Sander C, et al. Dictionary of immune responses to cytokines at single-cell resolution. Nature. 2023 Dec;625(7994):377–384. Available from: https://doi.org/10.1038/s41586-023-06816-9.

[108] Horvath LE, Werner T, Boucher K, Jones K. The relationship between tumor size and stage in early versus advanced ovarian cancer. Medical Hypotheses. 2013 May;80(5):684–687. Available from: https://doi.org/10.1016/j.mehy.2013.01.027.

[109] Tangjitgamol S, Manusirivithaya S, Sheanakul C, Leelahakorn S, Sripramote M, Thawaramara T, et al. Can we rely on the size of the lymph node in determining nodal metastasis in ovarian carcinoma? International Journal of Gynecological Cancer. 2003 May;13(3):297–302. Available from: https://doi.org/10.1046/j.1525-1438.2003.13192.x.

[110] Catron DM, Itano AA, Pape KA, Mueller DL, Jenkins MK. Visualizing the First 50 Hr of the Primary Immune Response to a Soluble Antigen. Immunity. 2004 Sep;21(3):341–347. Available from: https://doi.org/10.1016/j.immuni.2004.08.007.

[111] Kaech SM, Ahmed R. Memory CD8+ T cell differentiation: initial antigen encounter triggers a developmental program in naïve cells. Nature Immunology. 2001 May;2(5):415–422. Available from: https://doi.org/10.1038/87720.

[112] Zhang Y, Wallace DL, De Lara CM, Ghattas H, Asquith B, Worth A, et al. In vivo kinetics of human natural killer cells: the effects of ageing and acute and chronic viral infection. Immunology. 2007 Mar;121(2):258–265. Available from: https://doi.org/10.1111/j.1365-2567.2007.02573.x.

[113] Anaya JM, Shoenfeld Y, Rojas-Villarraga A, Levy RA, Cervera R. Autoimmunity: from bench to bedside [Internet]. El Rosario University Press; 2013.

[114] Jelley-Gibbs DM, Lepak NM, Yen M, Swain SL. Two Distinct Stages in the Transition from Naive CD4 T Cells to Effectors, Early Antigen-Dependent and Late Cytokine-Driven Expansion and Differentiation. The Journal of Immunology. 2000 Nov;165(9):5017–5026. Available from: https://doi.org/10.4049/jimmunol.165.9.5017.

[115] Darrasse-Jèze G, Bergot AS, Durgeau A, Billiard F, Salomon BL, Cohen JL, et al. Tumor emergence is sensed by self-specific CD44hi memory Tregs that create a dominant tolerogenic environment for tumors in mice. Journal of Clinical Investigation. 2009 Aug. Available from: https://doi.org/10.1172/JCI36628.

[116] Rubinstein MM, Grisham RN, Cadoo K, Kyi C, Tew WP, Friedman CF, et al. A phase I open-label study of selinexor with paclitaxel and carboplatin in patients with advanced ovarian or endometrial cancers. Gynecologic Oncology. 2021 Jan;160(1):71–76. Available from: https://doi.org/10.1016/j.ygyno.2020.10.019.

[117] Yeh CY, Aguirre K, Laveroni O, Kim S, Wang A, Liang B, et al. Mapping spatial organization and genetic cell-state regulators to target immune evasion in ovarian cancer. Nature Immunology. 2024 Aug. Available from: https://doi.org/10.1038/s41590-024-01943-5.

[118] Fucikova J, Kralikova P, Fialova A, Brtnicky T, Rob L, Bartunkova J, et al. Human Tumor Cells Killed by Anthracyclines Induce a Tumor-Specific Immune Response. Cancer Research. 2011 Jul;71(14):4821–4833. Available from: https://doi.org/10.1158/0008-5472.CAN-11-0950.

[119] Abdullah TM, Whatmore J, Bremer E, Slibinskas R, Michalak M, Eggleton P. Endoplasmic reticulum stress-induced release and binding of calreticulin from human ovarian cancer cells. Cancer Immunology, Immunotherapy. 2021 Nov;71(7):1655–1669. Available from: https://doi.org/10.1007/s00262-021-03072-6.

[120] Kim YO, Kim KT, Yoo JB, Cho SH, Hwang YY, Moon H, et al. Significance of Interleukin-2(IL-2), Interleukin-6(IL-6), and Tumor Necrosis Factor-a(TNF-a) in the Ascites of Ovarian Cancer. Korean Journal of Gynecologic Oncology and Colposcopy. 1996;7(1):1. Available from: https://doi.org/10.3802/kjgoc.1996.7.1.1.

[121] Sutton GJ, Poppe D, Simmons RK, Walsh K, Nawaz U, Lister R, et al. Comprehensive evaluation of deconvolution methods for human brain gene expression. Nature Communications. 2022 Mar;13(1). Available from: https://doi.org/10.1038/s41467-022-28655-4.

[122] Giuntoli RL, Webb TJ, Zoso A, Rogers O, Diaz-Montes TP, Bristow RE, et al. Ovarian cancer-associated ascites demonstrates altered immune environment: implications for antitumor immunity. Anticancer research. 2009;29(8):2875-84.

[123] Nowak M, Klink M, Glowacka E, Sulowska Z, Kulig A, Szpakowski M, et al. Production of Cytokines During Interaction of Peripheral Blood Mononuclear Cells with Autologous Ovarian Cancer Cells or Benign Ovarian Tumour Cells. Scandinavian Journal of Immunology. 2010 Feb;71(2):91–98. Available from: https://doi.org/10.1111/j.1365-3083.2009.02350.x.

[124] Monavarian M, Elhaw AT, Tang PW, Javed Z, Shonibare Z, Scalise CB, et al. Emerging perspectives on growth factor metabolic relationships in the ovarian cancer ascites environment. Seminars in Cancer Biology. 2022 Nov;86:709–719. Available from: https://doi.org/10.1016/j.semcancer.2022.03.004.

[125] Rabinovich A, Medina L, Piura B, Huleihel M. Expression of IL-10 in human normal and cancerous ovarian tissues and cells. European cytokine network. 2010;21(2):122-8.

[126] Sender R, Weiss Y, Navon Y, Milo I, Azulay N, Keren L, et al. The total mass, number, and distribution of immune cells in the human body. Proceedings of the National Academy of Sciences. 2023 Oct;120(44). Available from: https://doi.org/10.1073/pnas.2308511120.

[127] Rådestad E, Klynning C, Stikvoort A, Mogensen O, Nava S, Magalhaes I, et al. Immune profiling and identification of prognostic immune-related risk factors in human ovarian cancer. OncoImmunology. 2018 Nov;8(2):e1535730. Available from: https://doi.org/10.1080/2162402X.2018.1535730.

[128] Flores-Romo L. In vivo maturation and migration of dendritic cells. Immunology. 2001 Mar;102(3):255–262. Available from: https://doi.org/10.1046/j.1365-2567.2001.01204.x.

[129] Zandarashvili L, Sahu D, Lee K, Lee YS, Singh P, Rajarathnam K, et al. Real-time Kinetics of High-mobility Group Box 1 (HMGB1) Oxidation in Extracellular Fluids Studied by in Situ Protein NMR Spectroscopy. Journal of Biological Chemistry. 2013 Apr;288(17):11621–11627. Available from: https://doi.org/10.1074/jbc.M113.449942.

[130] Zhang Y, Thangam R, You SH, Sultonova RD, Venu A, Min JJ, et al. Engineering Calreticulin-Targeting Monobodies to Detect Immunogenic Cell Death in Cancer Chemotherapy. Cancers. 2021 Jun;13(11):2801. Available from: https://doi.org/10.3390/cancers13112801.

[131] Ruedl C, Koebel P, Bachmann M, Hess M, Karjalainen K. Anatomical Origin of Dendritic Cells Determines Their Life Span in Peripheral Lymph Nodes. The Journal of Immunology. 2000 Nov;165(9):4910–4916. Available from: https://doi.org/10.4049/jimmunol.165.9.4910.

[132] Kamath AT, Henri S, Battye F, Tough DF, Shortman K. Developmental kinetics and lifespan of dendritic cells in mouse lymphoid organs. Blood. 2002 Sep;100(5):1734–1741. Available from: https://doi.org/10.1182/blood.V100.5.1734.h81702001734_1734_1741.

[133] Dalod M, Chelbi R, Malissen B, Lawrence T. Dendritic cell maturation: functional specialization through signaling specificity and transcriptional programming. The EMBO Journal. 2014 Apr;33(10):1104–1116. Available from: https://doi.org/10.1002/embj.201488027.

[134] Takada K, Jameson SC. Self–class I MHC molecules support survival of naive CD8 T cells, but depress their functional sensitivity through regulation of CD8 expression levels. Journal of Experimental Medicine. 2009 Sep;206(10):2253–2269. Available from: https://doi.org/10.1084/jem.20082553.

[135] Hellerstein M, Hanley MB, Cesar D, Siler S, Papageorgopoulos C, Wieder E, et al. Directly measured kinetics of circulating T lymphocytes in normal and HIV-1-infected humans. Nature Medicine. 1999 Jan;5(1):83–89. Available from: https://doi.org/10.1038/4772.

[136] Rubtsov YP, Niec RE, Josefowicz S, Li L, Darce J, Mathis D, et al. Stability of the Regulatory T Cell Lineage in Vivo. Science. 2010 Sep;329(5999):1667–1671. Available from: https://doi.org/10.1126/science.1191996.

[137] Vukmanovic-Stejic M, Zhang Y, Cook JE, Fletcher JM, McQuaid A, Masters JE, et al. Human CD4+ CD25hi Foxp3+ regulatory T cells are derived by rapid turnover of memory populations in vivo. Journal of Clinical Investigation. 2006 Sep;116(9):2423–2433. Available from: https://doi.org/10.1172/JCI28941.

[138] Patel AA, Zhang Y, Fullerton JN, Boelen L, Rongvaux A, Maini AA, et al. The fate and lifespan of human monocyte subsets in steady state and systemic inflammation. Journal of Experimental Medicine. 2017 Jun;214(7):1913–1923. Available from: https://doi.org/10.1084/jem.20170355.

[139] Italiani P, Boraschi D. From Monocytes to M1/M2 Macrophages: Phenotypical vs. Functional Differentiation. Frontiers in Immunology. 2014 Oct;5. Available from: https://doi.org/10.3389/fimmu.2014.00514.

[140] Wu SY, Fu T, Jiang YZ, Shao ZM. Natural killer cells in cancer biology and therapy. Molecular Cancer. 2020 Aug;19(1). Available from: https://doi.org/10.1186/s12943-020-01238-x.

[141] Lotze MT, Matory YL, Ettinghausen SE, Rayner AA, Sharrow SO, Seipp CA, et al. In vivo administration of purified human interleukin 2. II. Half life, immunologic effects, and expansion of peripheral lymphoid cells in vivo with recombinant IL 2. The Journal of Immunology. 1985 Oct;135(4):2865–2875. Available from: https://doi.org/10.4049/jimmunol.135.4.2865.

[142] Lotze MT, Frana LW, Sharrow SO, Robb RJ, Rosenberg SA. In vivo administration of purified human interleukin 2. I. Half-life and immunologic effects of the Jurkat cell line-derived interleukin 2. The Journal of Immunology. 1985 Jan;134(1):157–166. Available from: https://doi.org/10.4049/jimmunol.134.1.157.

[143] Conlon P, Tyler S, Grabstein K, Morrissey P. Interleukin-4 (B-cell stimulatory factor-1) augments the in vivo generation of cytotoxic cells in immunosuppressed animals. Biotechnology therapeutics. 1989;1(1):31-41.

[144] van Deventer S, Elson C, Fedorak R. Multiple doses of intravenous interleukin 10 in steroid-refractory Crohn's disease. Crohn's Disease Study Group. Gastroenterology. 1997 Aug;113(2):383–389. Available from: https://doi.org/10.1053/gast.1997.v113.pm9247454.

[145] Huhn RD, Radwanski E, Gallo J, Affrime MB, Sabo R, Gonyo G, et al. Pharmacodynamics of subcutaneous recombinant human interleukin-10 in healthy volunteers*. Clinical Pharmacology; Therapeutics. 1997 Aug;62(2):171–180. Available from: https://doi.org/10.1016/S0009-9236(97)90065-5.

[146] Atkins MB, Robertson MJ, Gordon M, Lotze MT, DeCoste M, DuBois JS, et al. Phase I evaluation of intravenous recombinant human interleukin 12 in patients with advanced malignancies. Clinical cancer research: an official journal of the American Association for Cancer Research. 1997;3(3):409-17.

[147] Foon K, Sherwin S, Abrams P, Stevenson H, Holmes P, Maluish A, et al. A phase I trial of recombinant gamma interferon in patients with cancer. Cancer Immunology Immunotherapy. 1985 Dec;20(3). Available from: https://doi.org/10.1007/BF00205575.

[148] Saks S, Rosenblum M. Recombinant human TNF-alpha: preclinical studies and results from early clinical trials. Immunology series. 1992;56:567-87.

[149] Oliver JC, Bland L, Oettinger CW, Arduino MJ, McAllister S, Aguero S, et al. Cytokine kinetics in an in vitro whole blood model following an endotoxin challenge. Lymphokine and cytokine research. 1993;12(2).

[150] Tirado-Rodriguez B, Ortega E, Segura-Medina P, Huerta-Yepez S. TGF-β: An Important Mediator of Allergic Disease and a Molecule with Dual Activity in Cancer Development. Journal of Immunology Research. 2014;2014:1–15. Available from: https://doi.org/10.1155/2014/318481.

[151] Gallo-Oller G, Di Scala M, Aranda F, Dotor J. In: Transforming growth factor beta (TGF-β) activity in immuno-oncology studies. Elsevier; 2020. p. 129–172. Available from: https://doi.org/10.1016/bs.mie.2019.06.008.

[152] Medsafe New Zealand. Paclitaxel Ebewe Concentrate for Solution for Infusion; 2023. Available from: https://www.medsafe.govt.nz/profs/datasheet/p/PaclitaxelEbeweinj.pdf.

[153] Di Pasqua AJ, Goodisman J, Kerwood DJ, Toms BB, Dabrowiak JC. Modification of carboplatin by Jurkat cells. Journal of Inorganic Biochemistry. 2007 Oct;101(10):1438–1441. Available from: https://doi.org/10.1016/j.jinorgbio.2007.06.018.

[154] Calvert AH, Newell DR, Gumbrell LA, O'Reilly S, Burnell M, Boxall FE, et al. Carboplatin dosage: prospective evaluation of a simple formula based on renal function. Journal of Clinical Oncology. 1989 Nov;7(11):1748–1756. Available from: https://doi.org/10.1200/JCO.1989.7.11.1748.

[155] Donadio C, Lucchesi A, Ardini M, Cosio S, Gadducci A. Renal impairment in patients with ovarian cancer. European Journal of Obstetrics & Gynecology and Reproductive Biology. 2003 Feb;106(2):198–202. Available from: https://doi.org/10.1016/S0301-2115(02)00234-8.

[156] Dermitzakis EV, Kimiskidis VK, Lazaridis G, Alexopoulou Z, Timotheadou E, Papanikolaou A, et al. The impact of paclitaxel and carboplatin chemotherapy on the autonomous nervous system of patients with ovarian cancer. BMC Neurology. 2016 Oct;16(1). Available from: https://doi.org/10.1186/s12883-016-0710-4.

[157] Nurgalieva Z, Liu CC, Du XL. Chemotherapy use and risk of bone marrow suppression in a large population-based cohort of older women with breast and ovarian cancer. Medical Oncology. 2010 Apr;28(3):716–725. Available from: https://doi.org/10.1007/s12032-010-9512-5.

[158] Rachma B, Savitri M, Sutanto H. Cardiotoxicity in platinum-based chemotherapy: Mechanisms, manifestations, and management. Cancer Pathogenesis and Therapy. 2025 Mar;3(2):101–108. Available from: https://doi.org/10.1016/j.cpt.2024.04.004.

[159] ten Bokkel Huinink WW, van Warmerdam LJC, Helmerhorst TJ, Schaefers MCW, Beijnen IH, Rodenhuis S. Phase II study of the combination carboplatin and paclitaxel in patients with ovarian cancer. Annals of Oncology. 1997 Apr;8(4):351–354. Available from: https://doi.org/10.1023/a:1008219618331.

[160] Pignata S, Scambia G, Katsaros D, Gallo C, Pujade-Lauraine E, De Placido S, et al. Carboplatin plus paclitaxel once a week versus every 3 weeks in patients with advanced ovarian cancer (MITO-7): a randomised, multicentre, open-label, phase 3 trial. The Lancet Oncology. 2014 Apr;15(4):396–405. Available from: https://doi.org/10.1016/S1470-2045(14)70049-X.

[161] Dessai SB, Chakraborty S, Babu TVS, Nayanar S, Bhattacharjee A, Jones J, et al. Tolerance of weekly metronomic paclitaxel and carboplatin as neoadjuvant chemotherapy in advanced ovarian cancer patients who are unlikely to tolerate 3 weekly paclitaxel and carboplatin. South Asian Journal of Cancer. 2016 Apr;05(02):063–066. Available from: https://doi.org/10.4103/2278-330X.181629.

[162] Clamp AR, James EC, McNeish IA, Dean A, Kim JW, O'Donnell DM, et al. Weekly dose-dense chemotherapy in first-line epithelial ovarian, fallopian tube, or primary peritoneal cancer treatment (ICON8): overall survival results from an open-label, randomised, controlled, phase 3 trial. The Lancet Oncology. 2022 Jul;23(7):919–930. Available from: https://doi.org/10.1016/S1470-2045(22)00283-2.

[163] Chan JK, Brady MF, Penson RT, Huang H, Birrer MJ, Walker JL, et al. Weekly vs. Every-3-Week Paclitaxel and Carboplatin for Ovarian Cancer. New England Journal of Medicine. 2016 Feb;374(8):738–748. Available from: https://doi.org/10.1056/NEJMoa1505067.

[164] Katsumata N, Yasuda M, Isonishi S, Takahashi F, Michimae H, Kimura E, et al. Long-term results of dose-dense paclitaxel and carboplatin versus conventional paclitaxel and carboplatin for treatment of advanced epithelial ovarian, fallopian tube, or primary peritoneal cancer (JGOG 3016): a randomised, controlled, open-label trial. The Lancet Oncology. 2013 Sep;14(10):1020–1026. Available from: https://doi.org/10.1016/S1470-2045(13)70363-2.

[165] Duffull SB, Robinson BA. Clinical Pharmacokinetics and Dose Optimisation of Carboplatin. Clinical Pharmacokinetics. 1997 Sep;33(3):161–183. Available from: https://doi.org/10.2165/00003088-199733030-00002.

[166] Dessai SB, Chakraborty S, Babu TVS, Nayanar S, Bhattacharjee A, Jones J, et al. Tolerance of weekly metronomic paclitaxel and carboplatin as neoadjuvant chemotherapy in advanced ovarian cancer patients who are unlikely to tolerate 3 weekly paclitaxel and carboplatin. South Asian Journal of Cancer. 2016 Apr;05(02):063–066. Available from: https://doi.org/10.4103/2278-330X.181629.

[167] Clamp AR, James EC, McNeish IA, Dean A, Kim JW, O'Donnell DM, et al. Weekly dose-dense chemotherapy in first-line epithelial ovarian, fallopian tube, or primary peritoneal cancer treatment (ICON8): overall survival results from an open-label, randomised, controlled, phase 3 trial. The Lancet Oncology. 2022 Jul;23(7):919–930. Available from: https://doi.org/10.1016/S1470-2045(22)00283-2.

[168] Voest EE, van Houwelingen JC, Neijt JP. A meta-analysis of prognostic factors in advanced ovarian cancer with median survival and overall survival (measured with the log (relative risk)) as main objectives. European Journal of Cancer and Clinical Oncology. 1989 Apr;25(4):711–720. Available from: https://doi.org/10.1016/0277-5379(89)90208-3.

[169] William Hunter R, Alexander NDE, Patrick Soutter W. Meta-analysis of surgery in advanced ovarian carcinoma: Ismaximum cytoreductive surgery an independent determinant of prognosis? American Journal of Obstetrics and Gynecology. 1992 Feb;166(2):504–511. Available from: https://doi.org/10.1016/0002-9378(92)91658-w.

[170] Pritchard JR, Lauffenburger DA, Hemann MT. Understanding resistance to combination chemotherapy. Drug Resistance Updates. 2012 Oct;15(5–6):249–257. Available from: https://doi.org/10.1016/j.drup.2012.10.003.

[171] Barua S, Fang P, Sharma A, Fujimoto J, Wistuba I, Rao AUK, et al. Spatial interaction of tumor cells and regulatory T cells correlates with survival in non-small cell lung cancer. Lung Cancer. 2018 Mar;117:73–79. Available from: https://doi.org/10.1016/j.lungcan.2018.01.022.

[172] Maley CC, Koelble K, Natrajan R, Aktipis A, Yuan Y. An ecological measure of immune-cancer colocalization as a prognostic factor for breast cancer. Breast Cancer Research. 2015 Sep;17(1). Available from: https://doi.org/10.1186/s13058-015-0638-4.

[173] Mills C. M1 and M2 Macrophages: Oracles of Health and Disease. Critical Reviews in Immunology. 2012;32(6):463–488. Available from: https://doi.org/10.1615/critrevimmunol.v32.i6.10.

[174] Curtsinger JM, Schmidt CS, Mondino A, Lins DC, Kedl RM, Jenkins MK, et al. Inflammatory Cytokines Provide a Third Signal for Activation of Naive CD4+ and CD8+ T Cells. The Journal of Immunology. 1999 Mar;162(6):3256–3262. Available from: https://doi.org/10.4049/jimmunol.162.6.3256.

[175] Raphael I, Nalawade S, Eagar TN, Forsthuber TG. T cell subsets and their signature cytokines in autoimmune and inflammatory diseases. Cytokine. 2015 Jul;74(1):5–17. Available from: https://doi.org/10.1016/j.cyto.2014.09.011.